Generation of LOMU type alkali basalts in East Asia by melting and melt metasomatism of the asthenospheric mantle by a Paleoproterozoic subducted slab component

Dey Bidisha [1,2]

Corresponding Author

Email: bidisha-dey@hiroshima-u.ac.jp

Shibata Tomoyuki [1,2]

Yoshikawa Masako [1,2]

[1] Earth and planetary systems science program, Hiroshima University, 1-3-1 Kagamiyama, Higashi-Hiroshima City, Hiroshima, 739-8526, Japan

Ph: +81-082-424-7305

[2] Hiroshima Institute of Plate Convergence Region Research, Hiroshima University, 1-3-1 Kagamiyama, Higashi-Hiroshima City, Hiroshima, 739-8526, Japan

Ph: +81-082-424-7305

This is a pre-submission version of the manuscript published in the Journal of Petrology.

Please find the published article at https://doi.org/10.1093/petrology/egae104 (open access).

Generation of LOMU type alkali basalts in East Asia by melting and melt metasomatism of the asthenospheric mantle by a Paleoproterozoic subducted slab component

Bidisha Dey[1]*, Tomoyuki Shibata[1], Masako Yoshikawa[1]

[1]Earth and Planetary Systems Science Program, Hiroshima University, Higashi-Hiroshima, Japan

*bidisha-dey@hiroshima-u.ac.jp

ABSTRACT

The origin of alkali basalts with distinctive time-integrated low U/Pb (low μ, LOMU) from East Asia is controversial due to the complex geochemical and tectonic signatures reported from this region. We report new data on the petrology and geochemistry of the Higashi-Matsuura and Kita-Matsuura alkali basalts from southwest Japan, which confirms the presence of LOMU-type mantle components below the Japanese islands, similar to East Asian intraplate volcanoes. We use whole rock geochemistry and mineral chemistry to determine mantle melting, magma evolution conditions, and isotopic evolution of the LOMU mantle source. Petrological studies show that the Higashi-Matsuura alkali basalts (~3 Ma) were derived from a hydrous mantle source with ~950 µg/g H_2O, at a pressure of 1.9 to 2.3 GPa and a mantle potential temperature of ~1300 °C. Trace element modelling concludes that these basalts may have been generated through the hydrous upwelling and partial melting of the asthenospheric mantle containing ~15% dehydrated eclogitic component. These alkali basalts show $^{206}Pb/^{204}Pb$ values of 17.72 to 18.04 which are among the lowest values from southwest Japan. Relatively older (6–8 Ma) and shallower alkali basalts from the Kita-Matsuura area showing similar physicochemical characteristics, do not show LOMU-type isotopic trends. Trace element and Pb-Sr-Nd isotopic data indicate that the Higashi-Matsuura mantle component is similar to the extreme LOMU components reported from the northeast China alkali basalts, as well as the recently discovered Petit Spot volcanoes on the Pacific plate. We model the origin of the LOMU signature from the lowest reported Pb isotope ratios in East Asia, from the Xiaogulihe volcano in northeastern China. Our model suggests that at least two separate subduction events of marine sediments, at 1.8 Ga and 2.2 Ga, are required to explain the observed Pb isotopic variation in the East Asian region. Other LOMU type basalts from East Asia, including southwest Japan and Petit Spot, define a linear trend between the Xiaogulihe basalts and lithospheric mantle xenoliths. This suggests that the LOMU array in East Asia may have been formed by mixing between multiple ancient, subducted sediment components accumulated at the mantle transition zone for about 2 billion years, and its recent upwelling due to dehydration of the stagnant Pacific slab and related melting of the metasomatised asthenospheric mantle.

Keywords: Alkali basalts; East Asian mantle; LOMU; Southwest Japan; Eclogite melting

INTRODUCTION

Mantle geochemistry below the continents is difficult to determine due to the thick continental crust and its interactions with any upwelling magma. Nevertheless, attempts have been made to decipher the nature of the mantle beneath continental regions in order to understand the geochemical evolution of the Earth. The mantle below the East Asian region is of particular interest due to the complex geotectonic setting and unique geochemistry of volcanic rocks found in this region. Intraplate Cenozoic volcanism in northeast China and Korea comprising of ultrapotassic to alkaline basalts has been extensively studied and show ocean island basalt (OIB) like trace element patterns and an enriched mantle (EM 1), or LOMU [low-µ; Douglass *et al.*, (1999)] like radiogenic isotope ratios (Basu *et al.*, 1991; Menzies, 1995; Chen *et al.*, 2017; Sun *et al.*, 2017; Wang *et al.*, 2017; Choi *et al.*, 2020). However, the origin of this signature is

still ambiguous and thought to contain material from multiple components such as recycled sediments, oceanic crust, metasomatised asthenospheric mantle and the subcontinental lithospheric mantle (Choi *et al.*, 2006, 2020; Chen *et al.*, 2007; Kuritani *et al.*, 2009, 2011; Sun *et al.*, 2017; Wang *et al.*, 2017; Shi *et al.*, 2023). Some Cenozoic alkali basalts from southwest Japan showing OIB like trace element patterns have also been reported to contain low radiogenic Pb compared to arc basalts (Tatsumoto, 1969) and later linked to the enriched mantle 1 or EM 1 (Zindler and Hart, 1986) type mantle component (Tatsumoto and Nakamura, 1991). Nevertheless, the origin and evolution of such trace element and isotopic signature in southwest Japan has not been well defined. Although high $^{3}He/^{4}He$ in Takashima xenoliths from southwest Japan suggest a contribution from primitive lower mantle (Sumino *et al.*, 2000), plume from the lower mantle have not been observed in seismic studies in this area. Rather, the presence of the stagnant Pacific plate at the mantle transition zone (Fukao *et al.*, 1992; Richard and Iwamori, 2010; Zhao *et al.*, 2012a; Huang *et al.*, 2013), and a lack of a high $^{3}He/^{4}He$ in mantle xenoliths from northeast China (Chen *et al.*, 2007), suggests against any upwelling from the lower mantle below East Asia. Contribution from enriched mantle components (both EM 1 and EM 2) to the basalts of southwest Japan have been proposed in the past based on their radiogenic isotope geochemistry (Tatsumoto and Nakamura, 1991; Hoang and Uto, 2003, 2006). The source of the EM 1 or LOMU signature in East Asia has been suggested to originate from ancient subducted sediments based on Pb-Sr-Nd radiogenic and Mg-Ca-Zn stable isotope ratios (Eisele *et al.*, 2002; Kuritani *et al.*, 2011; Wang *et al.*, 2017; Choi and Liu, 2022; Shi *et al.*, 2023). Recent research suggests deep subduction of ancient carbonate sediments contributing to the time integrated low U/Pb bearing LOMU signature from northeast China, correlated to low $\delta^{26}Mg$, $\delta^{44/40}Ca$ and high $\delta^{57}Fe$, $\delta^{66}Zn$ (Li *et al.*, 2017; Sun *et al.*, 2017; Wang *et al.*, 2017; Liu and Li, 2019; Wei *et al.*, 2021; Shi *et al.*, 2023). However Choi and Liu (2022) argue for a Paleoproterozoic siliciclastic source for the EM 1 component in Changbaishan basalts, based on Pb-Mg-Zn isotope systematics with contribution from carbonated eclogite from the stagnant Pacific plate. Interestingly, similar isotopic signature with low radiogenic Pb have been reported from the recently discovered Petit Spot volcanoes (Fig. 1a) near the Japan Trench (Machida *et al.*, 2009; Liu *et al.*, 2020a; Hirano and Machida, 2022). The geochemical signatures of these basalts differ from the northeast China EM 1 type basalts to some extent and their genesis have been explained by mixing with ancient carbonated eclogites in the asthenospheric mantle (Liu *et al.*, 2020a). Hance, the possible heterogeneous distribution of multiple EM 1 or LOMU sources in the mantle below East Asia present an enigma for the evolution of the observed isotopic signature in this area. Until now, investigation on the source and nature of the continental EM 1 or LOMU mantle below East Asia has been focused on volcanoes from northeast China and Korea. In this study we investigate the mantle heterogeneity below southwest Japan using petrological, trace elemental, and Pb-Sr-Nd isotope ratios from Kita-Matsuura and Higashi-Matsuura alkali basalts. Furthermore, we re-evaluate the genetic model for EM 1/ LOMU signature from East Asia by modelling the trace element pattern and mixing and radiogenic evolution in Pb isotope space.

GEOTECTONIC BACKGROUND

The Japanese islands are situated at the junction of three major tectonic plates. The Pacific Plate is subducting beneath the Eurasian Plate at the Japan Trench and the Philippine Sea (PHS) Plate at the Izu-Bonine-Mariana Trench. The Philippine Sea Plate is in turn subducting beneath southwest Japan at the Nankai Trough and Ryukyu Trench (Fig. 1a). Arc and rear-arc volcanoes resulting from the subduction settings are seen all along Japan. Intraplate volcanoes unrelated to these subduction settings, are also found further west of the plate boundary in Jeju island, Xiaogulihe, Wudalianchi, Erkeshan, Changbaishan etc. (Kamata and Kodama, 1999; Choi *et al.*, 2006, 2020; Sakuyama *et al.*, 2014a; Shibata *et al.*, 2014; Sun *et al.*, 2014; Wang *et al.*, 2017; Kim *et al.*, 2019).

The subducted Pacific slab is stagnant at the 660 km discontinuity at the bottom of the upper mantle (Zhao *et al.*, 2012a), above which the Philippine sea plate is presently subducting below southwest Japan and has reached up to the Goto islands (Huang *et al.*, 2013). A buoyant hydrous plume generated from the stagnant Pacific slab is inferred to be present below the East Asian region (Richard and Iwamori, 2010; Huang *et al.*, 2013; Sakuyama *et al.*, 2013; Kuritani *et al.*, 2017).

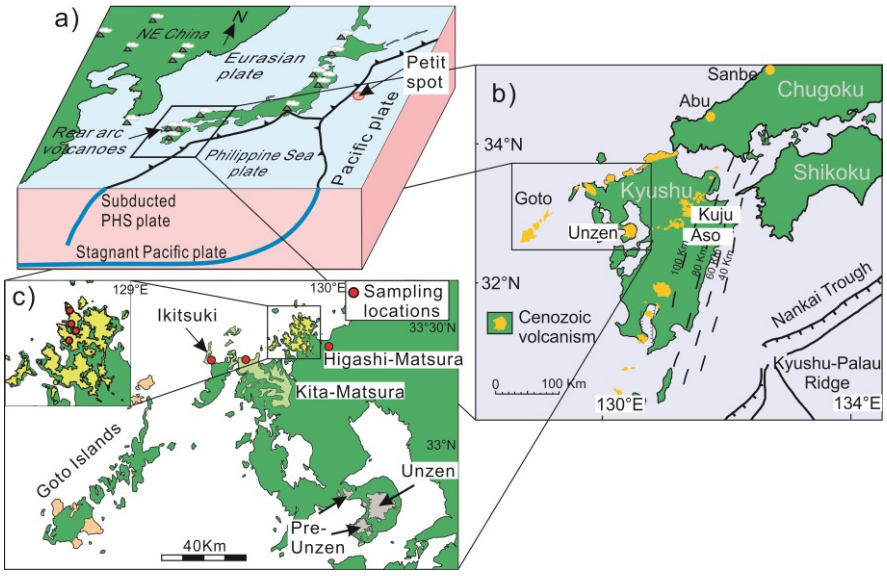

Fig 1. (a) Schematic diagram of the present-day tectonic setting in East Asia. The subducted Pacific plate is stagnated at the mantle transition zone below East Asia. (b) Location of southwest Japan arc and rear-arc volcanoes. Depth contour for the subducted PHS plate is shown as dashed lines. (c) Cenozoic rear arc volcanic fields from western Kyushu are differentiated by colour. Sampling locations in Kita-Matsuura and Higashi-Matsuura are indicated by red circles. Locations in Higashi-Matsuura are shown in inset, GPS coordinates are given in Table 1.

The southwest Japan arc extends NNE-SSW from southern Honshu (Daisen, Abu) to central Kyushu (Kuju) (Shibata *et al.*, 2014)(Fig. 1b), and Cenozoic volcanism from about 15 Ma to recent can be seen in the arc and rear-arc region. Subduction related volcanism prior to 15 Ma is the effect of the Pacific plate subducting beneath Eurasian plate and later volcanism (< 6 Ma) is related to the subduction of the Philippine Sea plate below Kyushu (Kamata and Kodama, 1999; Mahony *et al.*, 2011).

The samples analysed were sampled from the Kita-Matsuura and Higashi-Matsuura volcanic fields (Fig. 1c) of northwestern Kyushu, where basaltic volcanism is present from 6.11 to 8.63 Ma for Kita-Matsuura (Sakuyama *et al.*, 2009) and 2.92 to 3.01 Ma for Higashi-Matsuura (Nakamura *et al.*, 1986). The alkali olivine basalts in this study were collected from the Kita-Matsuura field in the Ikitsuki island and Tabiracho area, whereas the Higashi-Matsuura samples were collected near Genkaicho and Karatsushi areas of southwest Japan. Sample locations are shown in Fig. 1c, and GPS coordinates are represented in Table 1.

MATERIALS AND METHODS

Alkali basalts from Kita-Matsuura and Higashi-Matsuura were sampled from the field for petrological and geochemical studies. Thin sections were prepared, polished, and studied under polarising microscope and scanning electron microscope (SEM) at the Hiroshima University. Modal abundances were estimated by image analysis of ~1.5 cm^2 area of SEM images per thin section, using 'ImageJ' software. Chemical compositions of minerals were analysed using Electron Probe Microanalyzer (EPMA) of the model JEOL JXA-isp100 situated at the Hiroshima University. Samples were measured at an accelerating voltage of 15 kV and beam current of 10 nA. A probe diameter of 3 µm was used for olivine and clinopyroxene, and 5 µm was used for plagioclase. Mineral and oxide standards were used for calibration and data were obtained after ZAF correction.

All rock samples were crushed to coarse chips (≈0.5 cm^3) using a jaw crusher prior to whole-rock geochemical and Sr-Nd-Pb isotopic analyses. Fresh pieces without saw marks were handpicked for grinding and were rinsed with ethanol and Milli Q water in an ultrasonic bath to avoid surface contamination. The cleaned and dried rock chips were then ground to a grain-size of less than 200 mesh using a vibrating tungsten carbide puck mill. Glass beads were prepared, and major element and selected trace element compositions were determined using XRF (Rigaku ZSX-Primus II) installed at the Hiroshima University, following Kanazawa et al., (2001). Powdered samples were digested with HF, $HClO_4$ and HCl in a class 1000 clean room on a class 10 clean bench for trace element and isotopic analyses. Trace element compositions were determined after diluting the digested rock powders with 5% m/v HNO_3 and analysed in an inductively coupled plasma mass spectrometry (ICP-MS) of the model Thermo Scientific X Series-2 installed at the Hiroshima University (Chang *et al.*, 2002). Elemental separation for isotope ratio analysis was done from part of the digested sample. Pb, Sr and Nd were separated using

a sequential column chemistry method following Dey et al. (2023).

Pb-Sr-Nd isotope ratios were determined using a thermal ionisation mass spectrometer (TIMS) from Thermo Scientific (MAT-262), equipped with nine faraday cups, installed at the Hiroshima University. Instrumental mass fractionation was corrected by internal normalization for Sr and Nd with $^{86}Sr/^{88}Sr$ = 0.1194 (Birck, 1986) and $^{146}Nd/^{144}Nd$ = 0.7219 (Depaolo, 1988). Pb isotopic fractionation was corrected using double spike method with two separate measurements of unspiked and double spiked fractions (Compston and Oversby, 1969). Accuracy of measurement was confirmed by repeated measurements of isotope references for Sr, Nd and Pb. NIST SRM 987 provided an $^{87}Sr/^{86}Sr$ ratio of 0.710264 ± 0.000014 (2σ, n = 10) while La Jolla Nd standard provided a $^{143}Nd/^{144}Nd$ ratio of 0.511853 ± 0.000011 (2σ, n = 10). Double spike corrected values for NIST SRM 981 were measured as $^{206}Pb/^{204}Pb$ =16.9397 ± 0.0013; $^{207}Pb/^{204}Pb$ = 15.4972 ± 0.0013 and $^{208}Pb/^{204}Pb$ = 36.7187 ± 0.0024 (2σ) for an average of five measurements. Basaltic reference rock JB-2 from GSJ was prepared and measured alongside samples to ensure accuracy and reproducibility of measured data.

RESULTS

Petrography and mineral chemistry

All samples consist of fine-grained (< 500 μm), holocrystalline basalts; with olivine, clinopyroxene, and plagioclase microphenocrysts in a plagioclase, orthopyroxene, and opaque bearing groundmass (Fig 2). Little to no alteration was observed in hand specimens and thin sections.

One sample from Kita-Matsuura (TBR-2) contain large (~1 to 0.4 mm) olivine and clinopyroxene phenocrysts, in a medium grained (~500 to 200 μm), plagioclase-bearing groundmass with a total phenocryst abundance of ~31 vol%. Compositional zoning is visible in both olivine and clinopyroxene phenocrysts in polarising microscope and SEM (Fig. 2a, b). The forsterite content of olivine ranges from Fo_{85}- Fo_{87} in the core to ~Fo_{62} at the rim. Anorthite content for plagioclase microphenocrysts ranges from An_{59} to An_{65}. Olivine and clinopyroxene grains are clustered together and show resorbed grain boundaries in contact with plagioclase (Fig. 2a). Measured data is available in supplementary table S1.

Higashi-Matsuura basalts contain small to medium (50 to 500 μm) olivine grains (5 to 15 vol%) in a fine-grained plagioclase and orthopyroxene bearing groundmass along with small grains of Fe-Ti oxides (~5 vol%). Phenocryst phases are dominated by olivine with minor presence (<5 vol%) of clinopyroxene. Some olivine phenocryst grains are fractured and partially altered along fractures (Fig. 2b). Unlike the Kita-Matsuura samples, the olivine grains in Higashi-Matsuura samples do not show pronounced compositional zoning, with forsterite content ranging from Fo_{70} to Fo_{80}. Plagioclase microphenocrysts show anorthite contents ranging from An_{60} to An_{69}. A large plagioclase xenocryst (~1.5 mm) with resorbed grain boundary (Fig. 2c) shows anorthite content of An_{32} to An_{45}. Proportion of glass is non-existent or negligible in all samples, in agreement with previous observations by Nakamura et al. (1986). Presence of ultramafic xenoliths and xenocrysts has been reported in Higashi-Matsuura basalts (Nakamura *et al.*, 1986) but was not observed in the samples in this study.

Whole rock major and trace element compositions

Whole rock geochemical data of the measured samples are presented in Table 1. Measured data plot in tholeiitic to alkaline range in the basalt to trachy-basalt field in a total alkali vs silica diagram (Fig. 3a; Le Bas et al., 1986). CIPW Norms were calculated on anhydrous basis after redistribution of FeO* (Total Fe assumed as FeO) according to Fe^{+2}/Fe^{+3} = 0.8 (Table 2). Kita-Matsuura samples show 11 to 14% normative olivine (Ol) and 2.4 to 10.8% normative hypersthene (Hyp). Normative Ol and Hyp content are 12.6 to 16.2% and 0 to 5.6% for Higashi-Matsuura samples. One sample shows normative nepheline of 0.7%.

Samples were plotted in the geotectonic classification scheme for tholeiitic and alkaline rocks (Pearce and Cann, 1973) using immobile trace element data (Fig. 3b). Samples from Kita-Matsuura plot near the boundary of within-plate basalts and calc-alkaline basalts while the samples from Higashi-Matsuura plot in the within-plate basalt field. One sample from Higashi-Matsuura (HDO-2) was excluded from this classification due to anomalously high Y concentration (192 μg/g).

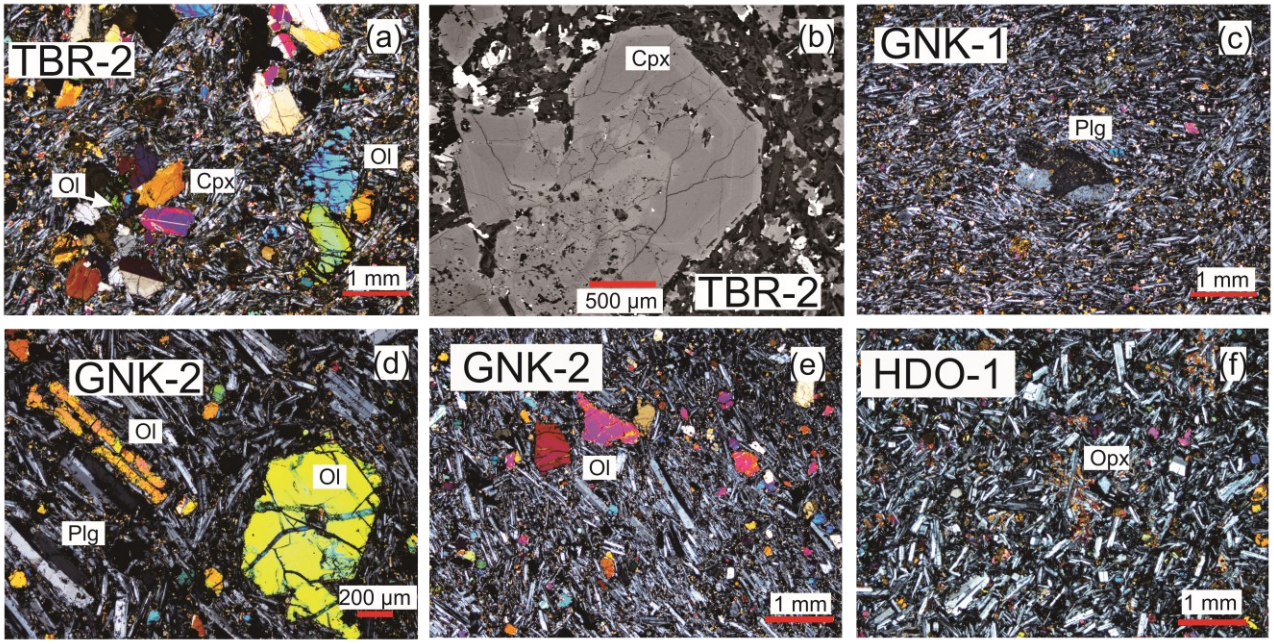

Fig 2. Representative thin sections of alkali basalts from Kita-Matsuura and Higashi-Matsuura. (a) Basalt from Kita-Matsuura (TBR-2) showing clustered clinopyroxene around olivine phenocrysts in plagioclase and orthopyroxene bearing groundmass. Olivine shows normal zoning identifiable by change in birefringence (b) Large clinopyroxene grain (TBR-2) showing compositional zoning in BSE (SEM). (c) Large (1.5 mm) plagioclase phenocryst in fine plagioclase and orthopyroxene bearing groundmass in sample (GNK-1) from Higashi-Matsuura (d) Euhedral and elongate olivine phenocrysts along with plagioclase microphenocrysts in sample (GNK-2) from Higashi-Matsuura. (e) Homogeneous olivine and plagioclase microphenocrysts in plagioclase-dominant groundmass visible in Higashi-Matsuura basalt. (f) Randomly oriented plagioclase laths and intergranular orthopyroxene seen in Higashi-Matsuura sample.

Primitive mantle normalized trace element diagram (Fig. 3c) and Chondrite normalized rare earth elements (REE) diagram (Fig. 3d) show similar patterns to ocean island basalts (OIB). High field strength element (HFSE) concentrations are significantly higher for all samples, with Nb ranging from 11 to 44 µg/g, compared to MORB or typical arc basalts (<5 µg/g). Depletion of HFSEs, which is a common trait for arc and rear-arc basalts are negligible for all the samples for Higashi-Matsuura (Nb/Nb* = 0.9 to 1.4) while the samples from Kita-Matsuura show weak depletion of Nb (Nb/Nb* = ~ 0.6). Ba, K, Pb and Sr show enriched pattern in trace element diagram compared to MORB. One sample from Kita-Matsuura (TBR-2) show high Ni (206 µg/g) and Cr concentration (479 µg/g) compared to other samples (<100 and <300 µg/g respectively) which may suggest relatively low mineral fractionation from primary magma. Chondrite normalized rare earth element pattern shows enrichment in light rare earths compared to heavy rare earths with $(La/Lu)_N$ values of 3–12.

Pb-Sr-Nd isotope compositions

$^{87}Sr/^{86}Sr$, $^{143}Nd/^{144}Nd$, $^{206}Pb/^{204}Pb$, $^{207}Pb/^{204}Pb$ and $^{208}Pb/^{204}Pb$ ratios are presented in Table-2, and isotope diagrams are plotted in Fig. 4. $^{87}Sr/^{86}Sr$ and $^{143}Nd/^{144}Nd$ isotope ratios range between 0.7039 and 0.7044 and 0.51267 and 0.51279 respectively which are enriched compared to the depleted mantle and MORB (Fig. 4a). Higashi-Matsuura samples show relatively more enriched Sr-Nd isotope ratios compared to Kita-Matsuura, while the reverse trend is seen for Pb isotope ratios. Measured data from Kita-Matsuura fall within previously reported values (Fig. 4) from Kita-Matsuura (Uto *et al.*, 2004; Sakuyama *et al.*, 2014b). Higashi-Matsuura samples show low radiogenic $^{206}Pb/^{204}Pb$ compared to previously reported data from Kyushu ($^{206}Pb/^{204}Pb$ = 17.8, Hoang and Uto, 2003), with $^{206}Pb/^{204}Pb$ between 17.72 to 18.04. $^{207}Pb/^{204}Pb$ and $^{208}Pb/^{204}Pb$ do not show such distinct difference from previously reported data, and range between 15.44 to 15.57 and 38.06 to 38.40 respectively.

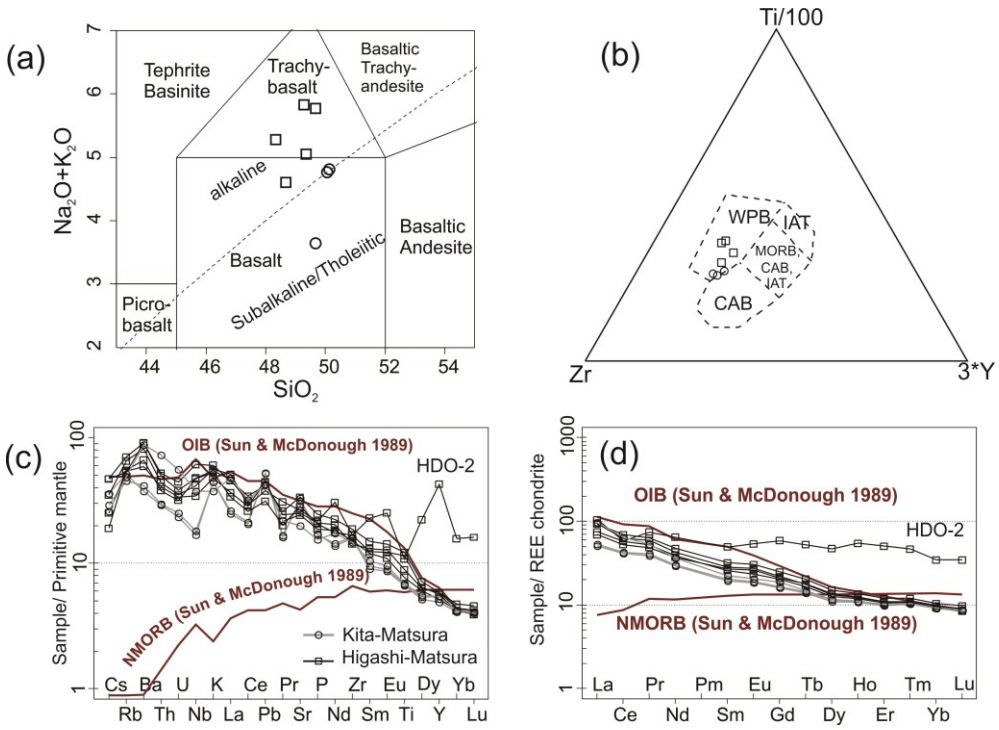

Fig 3. (a) Total alkali vs. silica diagram (La Bas et al 1986) for the measured samples. Circles and squares represent Kita-Matsuura and Higashi-Matsuura samples respectively. Kita-Matsuura basalts plot in the tholeiitic to alkaline basalt field, whereas Higashi-Matsuura samples plot in the alkaline basalt to trachy-basalt field. (b) Geotectonic classification of the analysed samples is plotted according to Pearce and Cann (1973). All samples belong to the within plate basalt group. One sample (HDO-2) has been excluded from this classification for having high Y/Nb ratio. (c) Primitive mantle normalized trace element pattern showing OIB like pattern for measured samples with minor Nb depletion for Kita-Matsuura samples and no depletion for Higashi-Matsuura samples. Fluid mobile elements (Ba, K, Sr, Pb) show enriched signature. HDO-2 shows anomalously high HREE and Y abundance compared to the other samples. (d) Chondrite normalized trace element pattern showing enrichment in LREE compared to HREE with no prominent Eu anomaly.

DISCUSSION

Physicochemical characteristics of the basaltic magma and inferred primary magma

Primary magma of basaltic nature is generally generated by decompression or fluid induced melting of the mantle (e.g. Tatsumi *et al.*, 1983; Wilson, 1989). Subsequent fractionation of minerals like olivine, clinopyroxene and plagioclase from the primary melt during ascent and cooling (Pearce, 1978; Tatsumi *et al.*, 1983), and assimilation of wall rock during ascent (DePaolo, 1981), may also change the composition of the magma before eruption and solidification. Such signatures are often decipherable from the petrographic features and chemical composition of the basalts. In the following section, we attempt to decipher the physicochemical nature of the basaltic magmas and their parent primary magmas.

Higashi-Matsuura

Higashi-Matsuura alkali basalts exhibit low SiO_2 (47.0 to 48.2 wt.%), with relatively high K_2O (1.5 to 1.9 wt.%) and Na_2O (2.9 to 4 wt.%) content (Table 1) compared to typical MORB or arc type basalts. MgO content varies between 4.4 to 7.4 wt.% with two samples (GNK-2 and Kaga-2) showing the highest abundances (~7.4 wt.%). These two samples also show the highest Ni (~100 µg/g) and Cr (217 to 280 µg/g) content suggesting that these may be the most primitive samples analysed for Higashi-Matsuura basalts. Tatsumi *et al.* (1983) suggested that primary magma in equilibrium with the mantle shows an FeO*/MgO ratio less than unity. However, both of the samples show FeO*/MgO >1 which suggests that these are not primary basalts, but some amounts of mineral fractionation have taken place from the primary magma. Arc and rear-arc basalts often

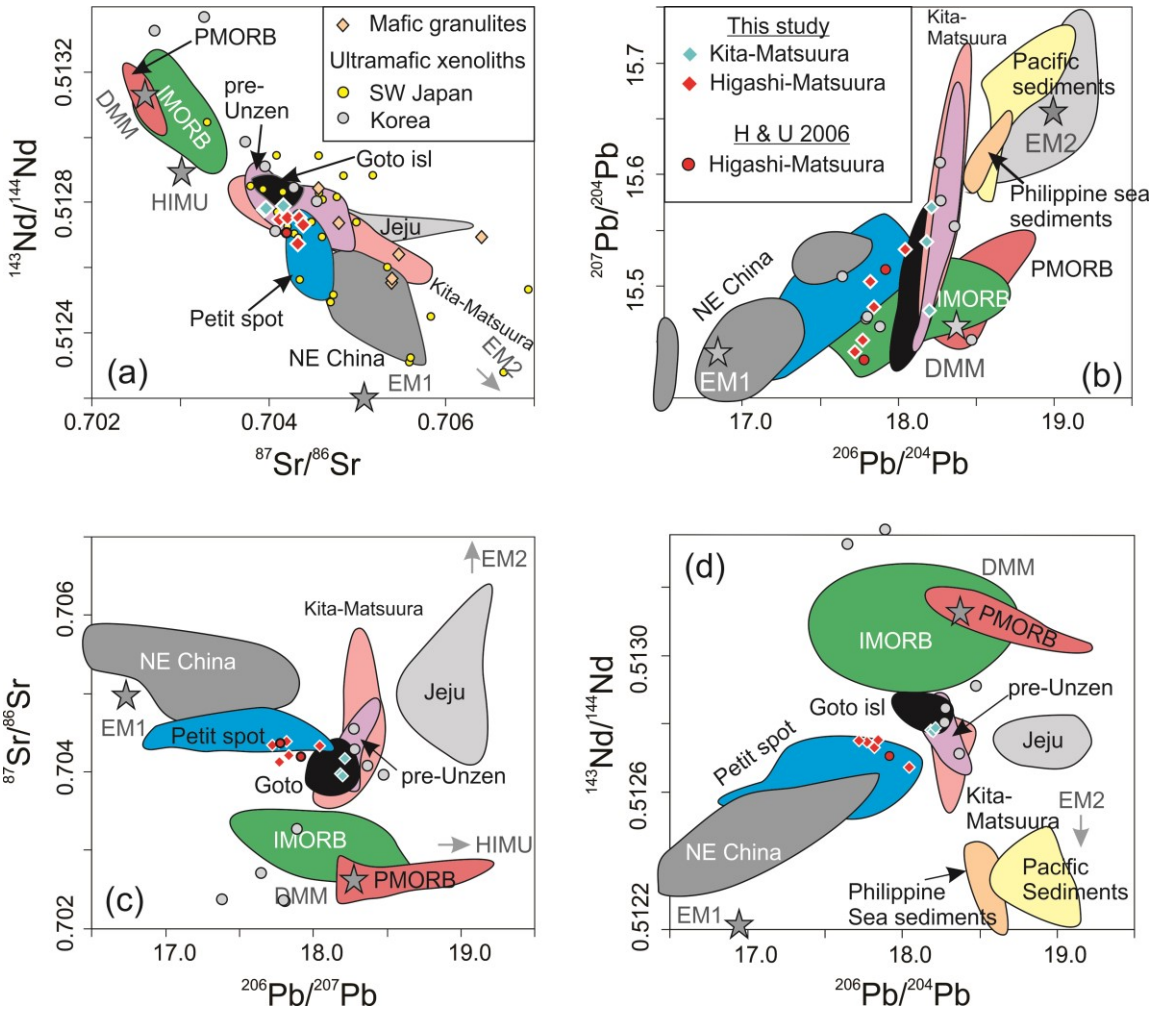

Fig 4. $^{87}Sr/^{86}Sr$, $^{143}Nd/^{144}Nd$, $^{206}Pb/^{204}Pb$, $^{207}Pb/^{204}Pb$ and $^{208}Pb/^{204}Pb$ ratios of measured samples compared to data from rear arc basalts of Kyushu, i.e., Goto island (Hoang *et al.*, 2013; Kuritani *et al.*, 2017), Unzen (Hoang and Uto, 2006; Sugimoto *et al.*, 2006), Kita-Matsuura (Uto *et al.*, 2004; Sakuyama *et al.*, 2014). Other components, i.e., northeast China intraplate basalts (Kuritani *et al.*, 2009; Sun *et al.*, 2014; Wang *et al.*, 2017), Jeju (Kim *et al.*, 2019), Petit spot (Liu *et al.*, 2020), Indian (IMORB) and Pacific (PMORB) type MORB (Gale *et al.*, 2013) and subducting sediments on the Philippine Sea plate and Pacific plate (Cousens *et al.*, 1994; Saitoh *et al.*, 2015) are also denoted in the diagrams. Data used for plotting can be found in supplementary Table S4. Sr-Nd data for mantle and lower crustal xenoliths from southwest Japan (Kagami *et al.*, 1993; Ikeda *et al.*, 2001; Senda *et al.*, 2007; Yoshikawa *et al.*, 2010) and Baengnyeong Island and Jogokni of Korea (Choi *et al.*, 2005) are shown. Two samples from Higashi-Matsuura reported by Hoang and Uto (2003) are shown as red circles. Mantle components DMM (Workman and Hart, 2005), EM 1, EM 2 and HIMU (Zindler and Hart, 1986) are plotted as star and approximate direction is indicated by arrow when outside the plotted area.

produce negative Eu anomaly in the chondrite normalised REE diagram due to fractionation of plagioclase in which Eu is strongly partitioned into plagioclase unlike other REEs. Assimilation of wall rock would produce the reverse effect and show a positive Eu anomaly in the chondrite normalised REE pattern. The absence of significant Eu anomaly (Eu/Eu* = 1.0 - 1.1) in the chondrite normalized REE diagram (Fig. 3d) suggests an insignificant plagioclase fractionation or crustal assimilation for these rocks. Mineral chemistry analysed for one of the samples (GNK-2) show a highest Fo# content of 80.5 as opposed to mantle olivine with Fo_{89}, suggesting that olivine fractionation may have taken place. One sample (HDO-2) deviate from the common trend with enriched heavy rare earth and Y. Rhabdophane, an Y bearing phase was reported from Higashi-Matsuura basalts from the Genkaicho region (Takai and Uehara, 2012) which may explain the enriched Y and HREE in this sample. This may indicate possible contamination during magma ascent or involvement of a distinct component in the source material. However, the Pb-

Sr-Nd isotope ratios do not show significant variation from the other samples of Higashi-Matsuura indicating that the Pb-Sr-Nd budget is not affected due to the contamination.

Crystallization conditions and water content of the basaltic magma was calculated for GNK-1 and GNK-2 using mineral chemistry data and clinopyroxene thermobarometry (Wang *et al.*, 2021) and hygrometry (Perinelli *et al.*, 2016). The pressure, temperature and H_2O content (Table S2) was simultaneously solved using the SOLVER function of Excel. Results from GNK-2 suggest that core of one relatively larger, euhedral Cpx was in equilibrium with a deeper (~0.6 GPa), hotter (1180 °C) and dryer (1.3 wt.% H_2O) melt, compared to smaller Cpx grains and rim of large grain (~0.2 GPa, 1090 °C, 2.0 wt.% H_2O). Cpx saturation temperature (eq. 34, Putirka, 2008) of 1181 °C, calculated for the magma composition equivalent to the whole rock at 0.6 GPa and 1.3 wt.% H_2O also agrees to the Cpx core temperature, suggesting that the core is in equilibrium with the whole rock composition. H_2O content in equilibrium with Cpx ranged from 1.9 to 2.3 wt.% for GNK-2, with an average of 2.0 wt.% for Cpx excluding one phenocryst core (1.3 wt.%). Cpx in groundmass of GNK-1 yielded equilibrium temperatures of ~1090°C at low pressure (<0.05 GPa) and 0.7 to 1.1 wt.% H_2O which indicates degassing at near surface conditions. Whole rock $Fe^{2+}/(Fe^{2+} + Fe^{3+})$ = 0.8 was selected following an estimates for ~2.0 wt.% H_2O by Kelley et al. (2006).

The most primitive samples free of xenocrysts, GNK-2 and Kaga-1 were selected for calculation of primary melt based on highest MgO content (~7.4) and high Ni and Cr abundances. It is assumed olivine has fractionated without significant clinopyroxene fractionation from the primary melt as Cpx phenocryst core is in equilibrium with the whole rock composition. The highest measured Fo# of olivine core ($Fo_{80.5}$) is fairly close to olivine in equilibrium with the whole rock composition (Fo_{85}) and mantle olivine (Fo_{89}), considering an olivine/ melt partition coefficient $(Fe^{2+}/Mg)^{olivine/melt}$ = 0.3 (Roeder and Emslie, 1970). Insignificant plagioclase fractionation can be inferred based on insignificant Eu anomaly in chondrite normalized REE diagram (Fig. 3d). The primary magma composition for these basalts were calculated using the olivine maximum fractionation model by addition of 0.5 wt.% equilibrium olivine (Roeder and Emslie, 1970) in each step following Tatsumi et al. (1983). Primary magma composition was determined for Kita-Matsuura samples after olivine addition up to equilibrium olivine with Fo_{90}, as the source mantle for Kyushu rear-arc basalts is likely to be refractory as demonstrated by mantle xenoliths hosted by Takashima and Fukuejima basalts (Sakuyama *et al.*, 2009). The calculated primary melts are obtained after addition of 13.5 and 16 wt.% equilibrium olivine for GNK-2 and Kaga-1 respectively. SiO_2 content of primary magma is 48.6 and 47.9 respectively. H_2O content of primary magma was calculated to be ~1.8 wt.% by assuming a constant H_2O/K_2O during crystal fractionation (Kuritani *et al.*, 2017). Composition of primary magmas and corresponding normative compositions are given in Table 3.

Kita-Matsuura

The three measured samples from Kita-Matsuura exhibit low SiO_2 (48.6 to 49 wt.%) and relatively high MgO content (6.7 to 9.5 wt.%). The FeO*/MgO ratios for these samples (1.02 to 1.27) suggests that these are not primary melt, rather may have formed by olivine fractionation from primary melt.

Crystallization pressure, temperature, and water content for basaltic melt were calculated for TBR-2, using Cpx thermobarometry and hygrometry similar to Higashi-Matsuura. Results suggest an H_2O content of ~2.3 wt.% ± 0.6 wt.% (2σ, n = 12) for calculated pressures ranging from 0.05 to 0.4 GPa and temperatures ranging from 1070 to 1130 °C. The Cpx saturation temperature of ~1165 °C for the whole rock composition calculated using eqn. 34 of Putirka (2008) also agree to the crystallization temperatures. Highest measured Fo# for olivine core is 87 which is in equilibrium with the whole rock composition considering an olivine/melt partition coefficient $(Fe^{2+}/Mg)^{olivine/melt}$ = 0.3 (Roeder and Emslie, 1970). Whole rock $Fe^{2+}/(Fe^{2+} + Fe^{3+})$ = 0.8 was selected following estimates for ~2.3 wt.% H_2O by Kelley et al. (2006). As the highest measured Fo# for olivine core is 87 which is fairly close to that of mantle olivine (Fo_{89}), we assumed that only olivine has fractionated from the primary magma. The primary magma composition for these basalts were calculated following a similar method as for Higashi-Matsuura basalts. Primary magma compositions for TBR-2 and

Ikitsuki samples were calculated to contain 49.6 to 49.7 wt.% SiO_2 after an addition of 6 to 11 wt.% equilibrium olivine. Water content of primary magma was calculated to be ~2.2 wt.% following similar methods to Higashi-Matsuura basalts. The relative uniformity in primary magma composition (e.g., SiO_2, MgO content; Table 4) of the three samples from Kita-Matsuura suggest that they are generated under similar conditions and undergone varied degrees of fractionation during upwelling.

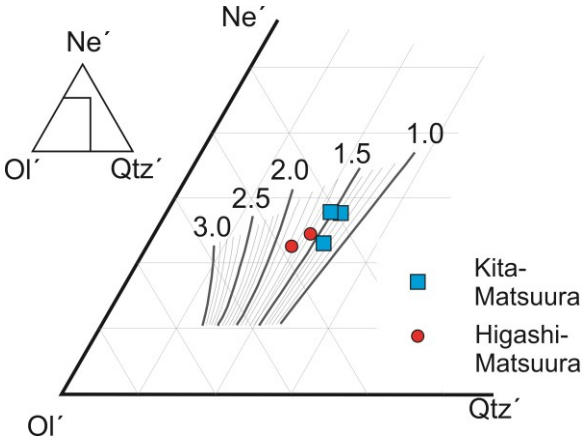

Fig 5. Ne′-Ol′-Qtz′ plot of normative components from calculated primary magma compositions. Projection scheme from Irvine and Baragar (1971), Ne′ = Ne + 0.6Ab; Qtz′ = Qtz + 0.4Ab + 0.25Opx; Ol′ = Ol + 0.75Opx. Sub-vertical lines from 1.0- 3.0 represent isopleths of melting pressure (GPa) after Sakuyama et al. (2009).

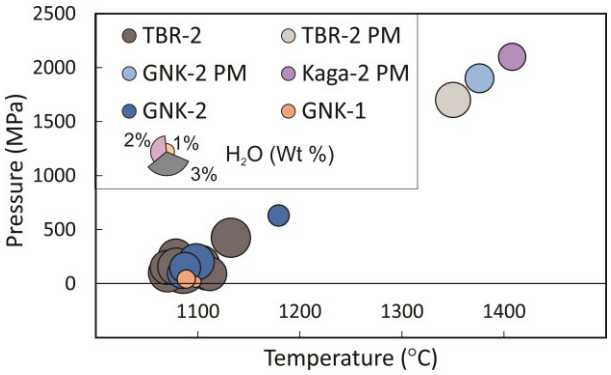

Fig 6. Pressure vs. temperature plot for Higashi-Matsuura (GNK-1, GNK-2, Kaga-2) and Kita-Matsuura (TBR-2). Primary magma (PM) data for GNK-2, Kaga-2 and TBR-2 represent estimated pressure and temperature of mantle melting. Other data points refer to pressure and temperature of Cpx crystallization after olivine fractionation. Diameter of circles represents H_2O content in the primary magma or equilibrium magma during Cpx crystallization. Data used for plotting can be found in supplementary Table S2.

Physicochemical conditions of the source mantle

Melting depths for primary magma generation were estimated using isopleths based on experimental data compiled by Sakuyama et al. (2009). Isopleths for mantle melting in the normative Ne′-Ol′-Qtz′ diagram of Irvine and Baragar, (1971) were used to determine depth of melting from calculated primary magma composition, following similar methods to Sakuyama et al. (2014b). Ne′, Ol′ and Qtz′ were calculated from the CIPW norm (Table 4) using calculated primary magma compositions following the formula Ne′ = nepheline + 0.6 × albite; Qtz′ = quartz + 0.4 × albite + 0.25 × orthopyroxene, and Ol′ = olivine + 0.75 × orthopyroxene (Irvine and Baragar, 1971). The results plotted in Fig. 5 show that the primary magmas of Kita-Matsuura basalts are plotted near the isopleths between 1.3 and 1.5 GPa, while the Higashi-Matsuura primary magmas are plotted at the 1.6 and 1.8 GPa isopleths. Corrections in melting pressure for water content were made according to the linear interpolation of $P^{wet} = P^{dry} + H_2O^{primary} \times 0.167$ (Sakuyama *et al.*, 2014b), resulting in a Equilibrium temperatures for primary magmas were estimated using the pMELTS mode (v5.6.1) in the online ENKI portal (Ghiorso *et al.*, 2002) at the calculated pressures and H_2O contents. The melting temperatures for Kita-Matsuura primary magmas were calculated to be between 1333 to 1358 °C while Higashi-Matsuura magmas yielded 1376 and 1408 °C for GNK-2 and Kaga-1 respectively. The calculated pressure and temperatures are plotted in Fig. 6, which show a linear trend connecting primary magma conditions and Cpx crystallization pressure temperatures after olivine fractionation.

The H_2O/Ce value of the source mantle is estimated to be 360 to 410 for Higashi-Matsuura and 410 to 630 for Kita-Matsuura, assuming that this value does not change significantly during mantle melting and fractional crystallisation (Michael, 1995). This value is higher than MORB (100- 250) (Michael, 1995) and depleted mantle (~150) (Salters and Stracke, 2004) but is lower than subduction zones (>750) (Cooper *et al.*, 2012) and Fukuejima basalts (~650) (Kuritani *et al.*, 2017). Degree of melting of the source mantle was calculated to be 4.08% for Higashi-Matsuura and 6.25% for Kita-Matsuura, assuming batch melting (Herzberg and O'hara, 2002) of a depleted source mantle composition of Salters and Stracke (2004) and 0.04 as.

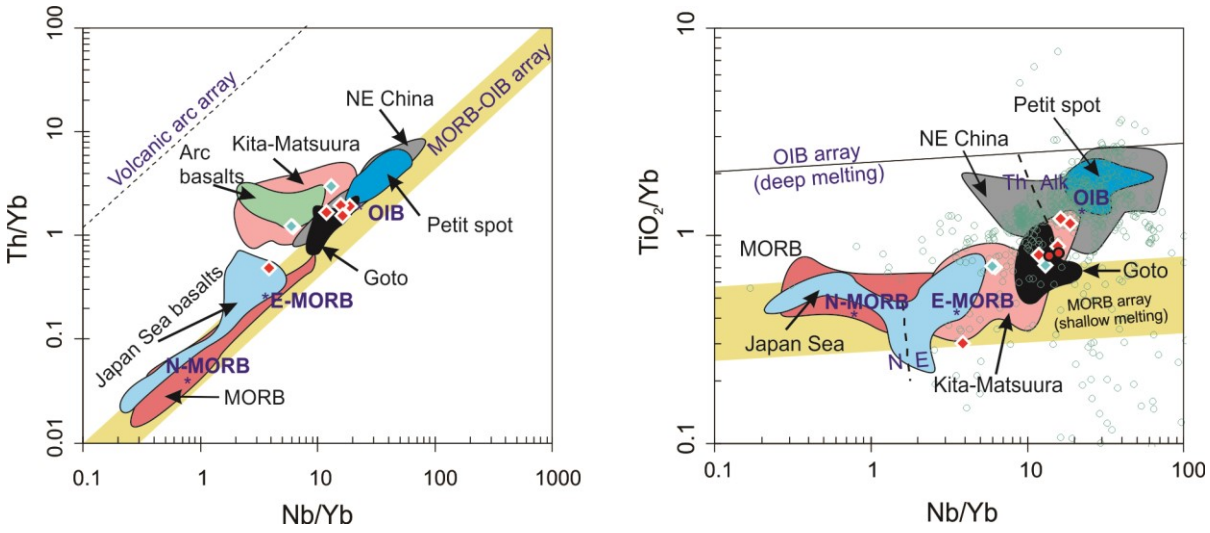

Fig 7. Basalt discrimination diagrams for southwest Japan and northeast China alkali basalts after Pearce (2008). (a) Discrimination between MORB-OIB type and arc type basalts in Th/Yb vs Nb/Yb diagram. Higashi-Matsuura alkali basalts fall in the MORB-OIB array along with northeast China, Petit Spot, and Goto island basalts. Kita-Matsuura basalts plot near the MORB-OIB array with an affinity towards the arc array. Arc basalts from southwest Japan, Daisen (Tamura et al., 2000), Aso, Himeshima and Futagoyama (Shibata et al., 2014) plot in between the MORB-OIB and arc array. (b) Discrimination between the MORB array and OIB array using TiO_2/Yb vs Nb/Yb diagram. Higashi-Matsuura basalts plot in a linear trend between the MORB and OIB array while the northeast China and Petit Spot plot near the OIB array and the Goto island basalts plot near the MORB array. MORB data (Gale et al., 2013) comprises of both I-MORB and P-MORB shown in figure 4. Japan sea basalts (Chen et al., 2015) also show similar character to MORB in both diagrams. Data used for plotting can be found in supplementary Table S4. Open circles in (b) denote pre-compiled data for EM1 type OIBs (Pitcairn-Gambier, Austral-Cook, Kerguelen, and Herd) from GEOROC database.

the bulk distribution coefficient of Ti (Kelley *et al.*, 2006). Melting was considered in the spinel stability zone based on estimated pressure and temperature of melting (Klemme and O'Neill, 2000). H_2O content in the source mantle was determined to be ~950 for Higashi-Matsuura and ~1600 µg/g for Kita-Matsuura source mantle, based on the bulk distribution coefficient of 0.012 of H_2O in the mantle (Kelley *et al.*, 2006) and batch melting of the depleted mantle. This water content is much higher than the MORB source mantle (50-200 µg/g) and correspond to the OIB source mantle (300- 1000 µg/g), and previously estimated water content (~1700 µg/g) in the sub-Kyushu mantle (Kuritani *et al.*, 2017). The data corroborates the hypothesis of a hydrous asthenospheric mantle below Kyushu (Sakuyama *et al.*, 2014b; Kuritani *et al.*, 2017) and East Asia (Chen *et al.*, 2015, 2017; Liu *et al.*, 2017). The results suggest that the Higashi-Matsuura basalts have been generated at a higher pressure and temperature and lower H_2O content compared to the Kita-Matsuura basalts.

Contribution from enriched and depleted mantle components

Nb/U (35 – 50) and Ce/Pb (16 – 21) ratios for Higashi-Matsuura which are similar to MORB and OIB values (47±10 and 25±5) indicate that these basalts are derived from the asthenospheric mantle with little contribution from the continental crust (Nb/U =10; Ce/Pb = 5)(Hofmann *et al.*, 1986). Relatively lower values (Nb/U = 22–24; Ce/Pb = 9–19) for Kita-Matsuura indicate a possible minor contribution from continental crust. Primitive mantle normalised trace element patterns (Fig. 3c) indicate an OIB-like trend for Kita-Matsuura and Higashi-Matsuura. Similar patterns are seen for Goto island (Hoang *et al.*, 2013; Kuritani *et al.*, 2017) and northeast China (Kuritani *et al.*, 2013; Sun *et al.*, 2017; Wang *et al.*, 2017), indicating that the mantle below this region is likely enriched in fluid mobile and immobile trace elements compared to MORB type mantle. A Th/Yb vs Nb/Yb plot (Fig. 7a) was used to distinguish between MORB/OIB type basalts and Arc type basalts following Pearce (2008). The figure suggests that the Higashi-Matsuura basalts lie close to the MORB-OIB array together with northeast China, Goto island and Petit Spot basalts. Measured Kita-Matsuura basalts

plot towards the volcanic arc array along with previously reported basalts from Kita-Matsuura and arc basalts from northeast and southwest Japan. A TiO_2/Yb vs Nb/Yb plot (Fig. 7b) showing the distinction between the MORB array and OIB array based on compiled data by Pearce (2008) suggests that the Higashi-Matsuura basalts plot towards the OIB array along with northeast China and Petit Spot basalts, whereas Goto Island and Kita-Matsuura basalts show a distribution from MORB to OIB type signature. The Nb enrichment [$Nb_N/(Th_N \times La_N)^{0.5}$] and HREE depletion $(Gd/Yb)_N$ of the basalts have been explored in Fig. 8, which show a nominal depletion to enrichment in Nb (Nb/Nb* = 0.9–1.4) and moderate depletion in HREEs [$(Gd/Yb)_N$ = 1.7–2.5] for Higashi-Matsuura alkali basalts, indicating an enriched source mantle similar to OIBs. The patterns are similar for Goto Island basalts while lower Nb/Nb* are observed for the measured Kita-Matsuura samples. Intraplate alkali basalts from northeast China and Petit Spot show higher HREE depletion [$(Gd/Yb)_N$ = 2–7.5] indicating deeper melting compared to the southwest Japan arc and rear arc samples. EM 1 type ocean island basalts (Pitcairn and Gambier, Austral- Cook, Kerguelen, and Herd; compiled geochemical data from GEOROC) are plotted in Fig. 7b and Fig. 8 and show similar geochemical characteristics to the southwest Japan rear arc basalts. These geochemical characters indicate that the mantle below southwest Japan may contain enriched domains similar to OIB type mantle, and the rear arc basalts are generated from a mixed domain of enriched and depleted source material.

The radiogenic isotopic ratios of Higashi-Matsuura basalts are enriched compared to the Indian and Pacific type MORB and depleted MORB mantle (DMM) as seen in Fig. 4. However, the measured ratios plot away from the general trend shown by Kyushu rear-arc basalts from Kita-Matsuura and pre-Unzen, and plot between Goto island and the northeast China alkali basalts (Fig. 4b, c, d). The Goto Island basalts plot on the same trend as Higashi-Matsuura albeit showing less enrichment in Pb-Sr-Nd isotope ratios. Ultramafic xenoliths from the subcontinental lithospheric mantle (SCLM) (Choi *et al.*, 2005) show similar Pb-Sr-Nd isotopic characteristics to Goto Island basalts in Fig. 4, which indicates that the Higashi-Matsuura and Goto Island basalts are likely to have originated from a LOMU type asthenospheric mantle domain similar to the northeast China basalts and interaction with the SCLM. Mafic and ultramafic xenoliths from southwest Japan (Kagami *et al.*, 1993; Ikeda *et al.*, 2001; Senda *et al.*, 2007; Yoshikawa *et al.*, 2010) are plotted in Fig. 4a and show $^{87}Sr/^{86}Sr$ and $^{143}Nd/^{144}Nd$ isotope ratios similar to southwest Japan back arc basalts. Hoang and Uto (2003, 2006) suggested that the SCLM below Kyushu is likely to be similar to EM 2 based on high Sr and low Nd isotopic ratios of Fukuoka basalts compared to MORB. Furthermore, the Pb-Sr-Nd isotopic data of mantle xenoliths from Korea reported by Choi *et al.* (2005) show similar ratios to Fukuejima basalts of Goto Island (Kuritani *et al.*, 2017), and do not show LOMU like values. Hance, it is unlikely that the SCLM is the source of the LOMU like signature.

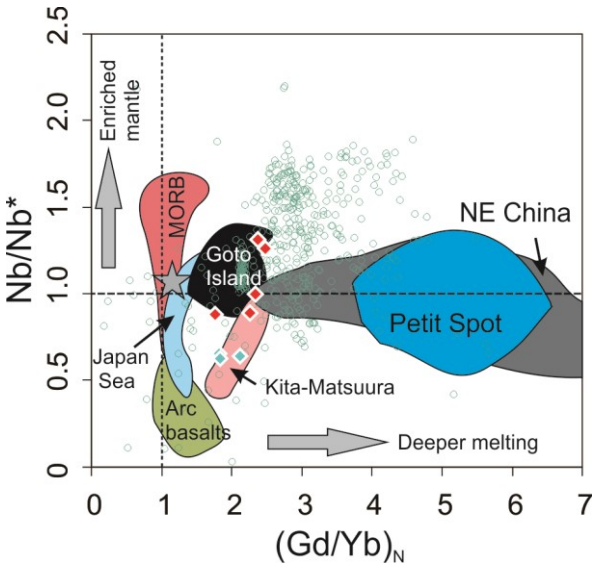

Fig 8. Nb/Nb* vs $(Gd/Yb)_N$ plot for measured and reported data from southwest Japan and northeast China. Nb* is calculated with respect to Th and La [$Nb/Nb^* = Nb_N/(Th_N \times La_N)^{0.5}$]. Normalisation is against primitive mantle values (Sun and McDonough, 1989). Average value for N-MORB (Gale *et al.*, 2013) is denoted by star symbol. Symbols for measured basalts are same as Fig. 4. Compiled data for EM 1 type OIBs are plotted similar to Fig. 7b.

These extremely low radiogenic Pb bearing alkali basalts from northeast China (Changbaishan, Wudalianchi, Nuominhe, Xiaogulihe, etc.) have been conclusively inferred to have been generated by asthenospheric melting triggered by hydrous upwelling from the stagnant Pacific slab and melt interaction with the SCLM based on mixing and evolution models in radiogenic (Pb-Sr-Nd) and stable (Fe-Mg-Ca-Zn) isotopic ratios (Kuritani *et al.*, 2011,

2013; Sakuyama *et al.*, 2014a; Wang *et al.*, 2017; Choi *et al.*, 2020; Shi *et al.*, 2023). Shi et al. (2023) suggested an eclogitic source, possibly derived from a subducted slab, for the EM 1 like signature in northeast China intraplate basalts based on high δ^{57}Fe and Zn/Fe ratios relative to MORB. Mixing between the LOMU source and SCLM has been proposed for alkali basalts from northeast China with a LOMU like signature (Wang *et al.*, 2017; Choi *et al.*, 2020). A similar mechanism of magma generation with melting of ancient subducted crust along with carbonate sediments is also proposed for Petit Spot on the Pacific slab based on low δ^{26}Mg data (Liu *et al.*, 2020a). On the other hand, based on whole rock geochemistry and mineral chemistry, it is proposed that ultrapotassic rocks from the Xiaogulihe volcano of northeast China have originated from the refractory lithospheric mantle which is metasomatised by carbonatitic melts (Weng *et al.*, 2022). A similar asthenospheric mantle source for the Higashi-Matsuura basalts can be speculated based on the similarity in trace element and Pb-Sr-Nd isotope ratios in the measured basalts and Northeast China alkali basalts.

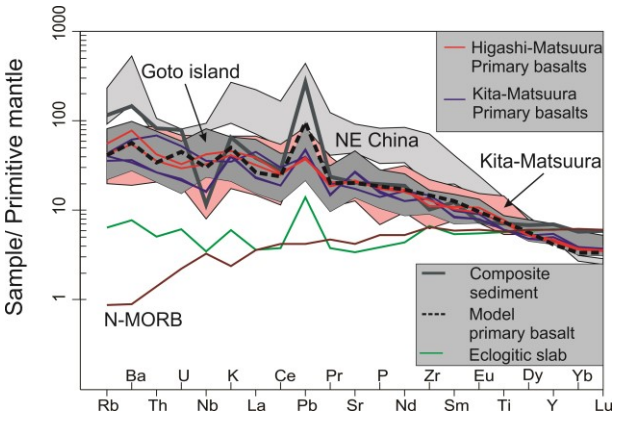

Fig 9. Modelled trace element pattern of partial melting of the asthenospheric mantle metasomatized by eclogitic slab shown as dashed line. The model has been fitted to be closest to the primary melt of Higashi-Matsuura basalt GNK-1. Primary melts calculated in this study from Kita-Matsuura and Higashi-Matsuura are shown as blue and red lines respectively. Subducting dehydrated composite sediments (85% GLOSS II + 15% carbonate sediments) trace element pattern is shown as thick grey line. Bulk eclogitic slab (5% composite sediments + 95% dehydrated MORB) is shown as green line. Data used for plotting can be found in supplementary Table S3. Trace element patterns for alkali basalts from Kitamatsuura, Goto island and northeast China are shown as shaded areas.

In order to test the hypothesis of eclogite melting in the asthenospheric mantle, we attempted to model the observed trace element patterns of the Higashi-Matsuura alkali basalts using the Ocean Basalt Simulator (OBS 1) of Kimura and Kawabata (2015). The OBS 1 simulates an upwelling mantle plume consisting of the depleted asthenospheric mantle and a relatively enriched eclogitic component and partial melting during upwelling. The partial melt from the eclogitic slab metasomatises the asthenospheric mantle and the metasomatised asthenospheric mantle subsequently melts to produce the observed primary basalts. We have assumed a subducted eclogitic slab consisting of 5% dehydrated sediments and 95% dehydrated oceanic crust with MORB composition in the depleted asthenospheric mantle (Table S3). The sediment composition was modelled to contain 85% of GLOSS II (Plank, 2014), with 15% carbonate-rich sediments with a similar composition to the sediment column at Central America (Plank, 2014). The composition of the modelled accumulated melt at the lithosphere-asthenosphere boundary is then compared to the primary magma composition of the target basalts. The mantle potential temperature, pressure at final melting, and proportion of eclogitic component were varied using Monte Carlo simulation to obtain best fit values to the primary magma composition of GNK-2. The results suggest a mantle potential temperature of ~1300 °C with a melt accumulation pressure of 2.3 GPa and ~15% eclogitic component in the mantle plume. Water content of the source mantle was assumed to be 750 ppm (limit for OBS 1 is 800 ppm) resulting in a 1.9 wt.% H_2O in the modelled primary basalts which matches to the calculated values from mineral chemistry (1.8%). The modelled trace element pattern is shown in Fig. 9 along with patterns for calculated primary magmas from this study and ranges for reported Kita-Matsuura, Goto Island, and Northeast China. The figure shows that the model matches the calculated primary basalts from Higashi-Matsuura and is within the range reported from Kita-Matsuura and Goto island.

The estimated pressure and mantle potential temperature are similar to previous estimates by Kuritani *et al.* (2017) for Goto Island using the pMELTS model. The mantle potential temperature is also within the range (1150 – 1350 °C) for subduction zone magmas generated by fluid-fluxed melting (Lee *et al.*, 2009). Melting of the enriched asthenospheric

mantle (~2.5 GPa) facilitated by hydrous upwelling over the stagnant Pacific slab has been proposed by many researchers in the field based on the geochemical characteristics of the basaltic magma (Kuritani *et al.*, 2011, 2013, 2017, 2019; Sakuyama *et al.*, 2014b, 2014a; Sun *et al.*, 2014; Chen *et al.*, 2017; Wang *et al.*, 2017; Choi *et al.*, 2020). The estimated melting pressures for the Kita-Matsuura and Higashi-Matsuura basalts indicate that they were generated from the bottom of the lithosphere to the top of the asthenospheric mantle, considering that the lithosphere-asthenosphere boundary is located at a depth of 60-65 km (~1.8 GPa) beneath northern Kyushu (Li, 2010). A 3D P-wave velocity model by Huang et al. (2013) shows a low velocity zone below western Kyushu at a depth of 60 - 200 km. Previous research by Sakuyama et al. (2014b) from Kita-Matsuura reported primary magma water contents of 0.2 to 2.3 wt.%, melting pressures of 1.5 to 2.8 GPa and temperatures of 1350 to 1500 °C. Relatively younger (<1 Ma) alkali basalts from Fukuejima have also been reported to have formed at a melting pressure of 1.8 to 2.6 GPa and 1285 to 1345 °C (Kuritani *et al.*, 2017) suggesting continuous mantle melting near the lithosphere-asthenosphere boundary for over 8 million years. Given the hydrous nature of the mantle source, coupled with melting in the upper part of the asthenospheric mantle, it is likely that a hydrous upwelling is responsible for the magmatism in this area. A similar explanation from previous studies from western Kyushu, which reported progressive, fluid fluxed melting of the asthenospheric mantle due to upwelling from the hydrous transition zone since the late Miocene (Sakuyama *et al.*, 2009, 2014b; Kuritani *et al.*, 2017), is consistent with this hypothesis. Kuritani et al., (2017) suggest that multiple phases of hydrous upwelling and mantle melting have occurred in Southwest Japan since the stagnation of the Pacific plate at the mantle transition zone. Considering the spatial distance and temporal separation between Kita-Matsuura (~6 to 8 Ma), Higashi-Matsuura (~3 Ma) and Fukuejima (0.5 Ma), it is likely that all of these volcanisms are separate events of hydrous upwelling and/or melting of the metasomatised asthenospheric mantle.

Origin of LOMU component in the East Asian mantle

The time-integrated low U/Pb signature of East Asian basalts has been extensively explored in previous studies. $\delta^{26}Mg$ ratios from Northeast China alkali basalts are correlated with K_2O content as well as $^{206}Pb/^{204}Pb$ suggesting that the source of correlated low radiogenic Pb and high radiogenic Sr is likely to be ancient carbonate sediments subducted into the mantle ~2 billion years ago (Kuritani *et al.*, 2011, 2017; Sun *et al.*, 2014, 2017; Wang *et al.*, 2017). This would have led to the time-integrated low U/Pb ratios (low μ or LOMU) in the generated basalts. Several studies from this area (Kuritani *et al.*, 2011, 2017; Sakuyama *et al.*, 2014a, 2014b; Sun *et al.*, 2014, 2017; Wang *et al.*, 2017) suggest that a region metasomatised by ancient sediments is present above the mantle transition zone in the asthenospheric mantle. Melting induced by dehydration from the stagnant Pacific slab below East Asia is responsible for transporting material from the deep metasomatised mantle and producing LOMU like isotopic signature in the Northeast China region. Considering the trace element model discussed in the previous section (Fig. 9), and a similar isotopic trend visible for the alkali basalts from Kyushu (Fig. 10), it is likely that the LOMU trend in southwest Japan may have originated by the mixing of metasomatised asthenospheric melt and the subcontinental lithospheric mantle, similar to that in Northeast China. The current study confirms the presence of a LOMU type isotopic signature below southwest Japan, suggesting that the metasomatised zone may be distributed throughout the mantle transition zone below East Asia. The absence of such isotopic signatures in other regions such as Kita-Matsuura and pre-Unzen may suggest that the asthenospheric mantle is isotopically heterogeneous below southwest Japan, or that another component (e.g., EM 2 type SCLM) is influencing the isotopic ratios, minimising the effect of the LOMU signature.

The source and origin of the LOMU signature has been discussed by various researchers and speculated to have originated either in the subcontinental lithospheric mantle (SCLM) (Basu *et al.*, 1991; Zhang *et al.*, 1995; Zou *et al.*, 2003) or in the asthenospheric mantle (Kuritani *et al.*, 2011, 2017; Sakuyama *et al.*, 2014a; Wang *et al.*, 2017) based on various geochemical parameters. Recent research correlating low $\delta^{26}Mg$, $\delta^{44/40}Ca$, and high $\delta^{57}Fe$, $\delta^{66}Zn$ to low radiogenic Pb have effectively established the origin of the Northeast China LOMU signature to be from an ancient, subducted carbonate-sediment rich region in the asthenospheric mantle

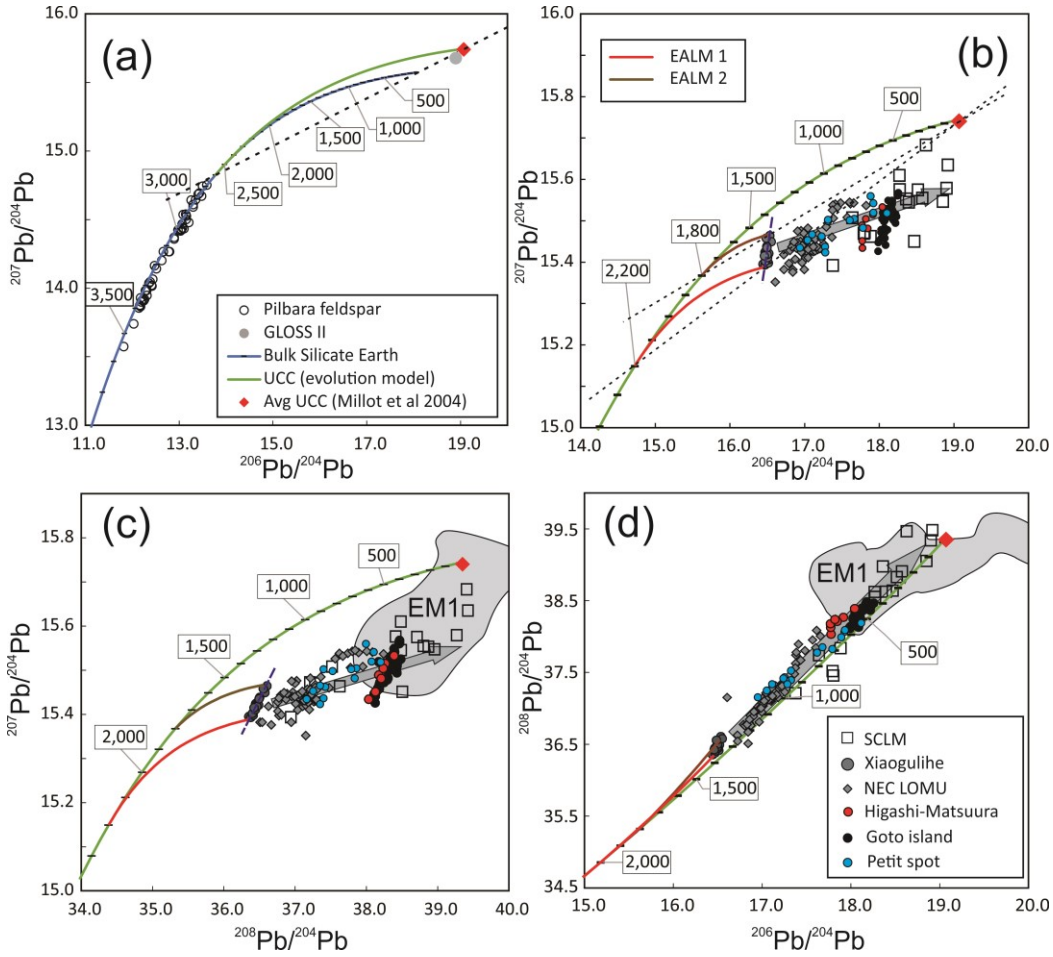

Fig 10. Pb isotopic evolution model and mixing model for East Asian Low μ (EALM) basalts. Numbers in boxes represent age in Ma. (a) Evolution model for Bulk silicate Earth (BSE) and average upper continental crust (UCC). BSE model is taken from Maltese and Mezger (2020). Pb isotopic ratios of Archean feldspars from Pilbara craton are taken from Hartnady et al. (2022). UCC evolution model is calculated using average composition from Millot et al. (2004) and corresponding μ and κ of 10.6 and 4.05 respectively for a time of fractionation of 2.6 Ga. Pb isotope ratio for global subducting sediments (GLOSS-II; Plank 2014) plots near the estimate for average UCC and falls on the isochron for UCC. (b) Model evolution for two low μ end members (EALM-1 and EALM-2) for Xiaogulihe ultrapotassic rocks. Numerical data used for modelling and plotting can be found in supplementary Table S5. Linear trend in Xiaogulihe data is represented by blue dashed line. Model age for these two subducting sediment components were estimated to be 2.2 and 1.8 Ga. Corresponding μ were calculated as 4.26 and 2.8 respectively. (c) and (d) shows same components w.r.t $^{208}Pb/^{204}Pb$. κ for EALM-1 and EALM-2 were calculated as 4.0 and 4.75 respectively. Pb isotopic data for Xiaogulihe is from Sun et al. (2014) Other samples from northeast China (Wudalianchi, Nuominhe, Erkeshan, Keluo, Changbaishan) are from Wang et al. (2017) and references therein, and Kuritani et al. (2009); Petit spot basalts are from Liu et al. (2020); Higashi-Matsuura basalts are from this study and Hoang et al. 2013 and Goto island basalts are taken from Kuritani et al. 2017. Data from subcontinental lithospheric mantle (SCLM) xenoliths are from Choi et al. (2005). EM1 type OIB data compiled from GEOROC (Pitcairn-Gambier, Astral-Cook, Kerguelen and Herd) are shown as grey area.

(Sun *et al.*, 2017; Wang *et al.*, 2017; Liu *et al.*, 2020b; Wei *et al.*, 2021; Shi *et al.*, 2023). A Pb isotope evolution model for development of this signature was reported by Wang et al. (2017), suggesting the subduction of carbonate sediments at 2.2 Ga and subsequent evolution in the mantle with low U/Pb ratios to develop the extreme LOMU ratios for this area. This model also explains the linear trend for the East Asian LOMU basalts as a mixing between a LOMU component and an EM 1 type signature shown by OIBs, which can be seen in Fig. 10b, c & d, but is not consistent with the Nd-Sr isotope ratios of the East Asian basalts and the EM 1 component (Fig. 4). Rather, based on the SCLM isotopic signatures reported by

Choi et al. (2005) and plotted in Fig. 4 and Fig. 10, it is more likely to be the mixed component in East Asian LOMU basalts. Furthermore, this model is unable to explain the linear trend seen within the Xiaogulihe samples (Fig. 10b, c, Fig. 11), which are the extreme endmembers of the East Asian LOMU signature. A 3-dimensional plot for Pb isotopes in Fig. 11 shows that ultrapotassic rocks and the LOMU type alkali basalts from northeastern China (Xiaogulihe, Nuominhe, Erkeshan, Keluo, Wudalianchi, Changbaishan) define a planar distribution in $^{206}Pb/^{204}Pb$- $^{207}Pb/^{204}Pb$- $^{208}Pb/^{204}Pb$ space with the Xiaogulihe ultrapotassic rocks defining one edge and the SCLM at the other end. Samples analysed from Higashi-Matsuura (this study), alkali basalts from petit spot near the Japan Trench (Liu *et al.*, 2020a), and Goto islands (Hoang *et al.*, 2013; Kuritani *et al.*, 2017) also fall in the same trend (Fig. 10, 11). This suggests at least two different components are mixing to provide the low radiogenic Pb signature for this region. The EM 1 type OIBs lie on the higher radiogenic Pb side of the linear trend, indicating a distinct LOMU component is responsible for the low radiogenic Pb signature. Therefore, we define the LOMU type Cenozoic alkali basalts and ultrapotassic rocks from northeastern China, Korea, and Southwest Japan as 'East Asian low μ' (EALM) basalts and attempt to re-evaluate the Pb isotopic evolution model to explain these signatures.

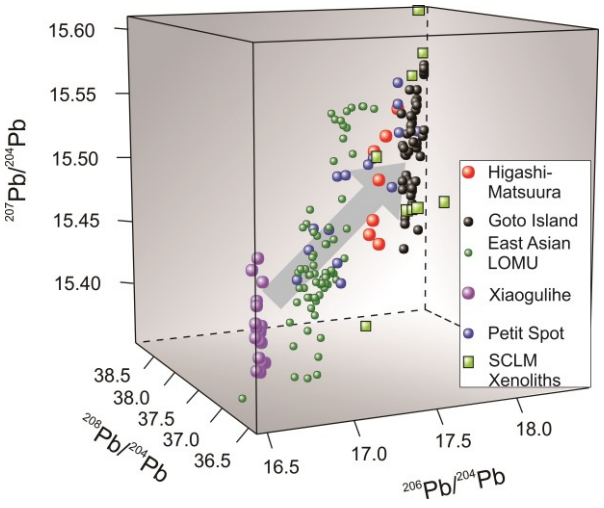

Fig 11. Pb isotopic data from measured and compiles samples from northeast China and southwest Japan alkali basalts and subcontinental lithospheric mantle plotted in $^{206}Pb/^{204}Pb$- $^{207}Pb/^{204}Pb$- $^{208}Pb/^{204}Pb$ 3D plot. References for compiled data is same as Fig. 10. The plotted data shows a planar distribution and mixing relation between Xiaogulihe and SCLM xenoliths.

Pb isotopic model

Pb is an element consisting of three radiogenic and one non radiogenic isotope in nature. ^{206}Pb and ^{207}Pb are the radiogenic daughters of ^{238}U and ^{235}U respectively, while ^{208}Pb is the radiogenic daughter of ^{232}Th. ^{204}Pb, the least abundant of the four, is considered non-radiogenic in geologic timescales and is used as the denominator to express Pb isotope ratios. Radiogenic isotope ratios in a closed system depend only on the parent-daughter ratio, the initial ratio of the daughter isotopes, and time. Although no natural system is truly closed, we can consider a component to be closed for the purpose of geochemical modelling, unless significant mixing or fractionation between parent and daughter elements has occurred during the considered time. The fact that two different variables, i.e., $^{206}Pb/^{204}Pb$ and $^{207}Pb/^{204}Pb$ are dependent on three parameters, i.e., the U/Pb ratio denoted as μ, the initial Pb isotope ratios, and time, makes the Pb isotopic system a robust tool for modelling mixing and evolution models of mantle components.

Pb isotopic evolution of the earth has been modelled by various researchers in order to explain the present-day crustal and mantle isotope ratios (Stacey and Kramers, 1975; Rudnick *et al.*, 1990; Connelly and Bizzarro, 2016; Maltese and Mezger, 2020; Fang *et al.*, 2022; Hartnady *et al.*, 2022). We use a Pb isotope evolution model for the bulk silicate Earth, proposed by Maltese and Mezger (2020) as the starting point to develop the LOMU signature of East Asia. Assuming that the LOMU signature is generated from ancient, subducted sediments (Eisele *et al.*, 2002; Wang *et al.*, 2017), these sediments are likely to have had similar Pb isotopic ratios to the upper continental crust (UCC) at the time of subduction. Therefore, we first determine the Pb isotopic evolution of the average UCC which has fractionated from the BSE. Although the UCC has been generated and accumulated in phases since 4.3 Ga (Condie, 2021; Hartnady *et al.*, 2022), we assume that the present day average UCC (Millot *et al.*, 2004) can be traced back to calculate the Pb isotopic ratios of the average UCC at any earlier time. The line connecting the present-day BSE and the present-day average UCC defines an isochrone on the $^{206}Pb/^{204}Pb$ vs $^{207}Pb/^{204}Pb$ diagram (Fig. 10a). This line intersects the BSE curve at 2.6 Ga which can be considered as a model age of the average UCC. The initial $^{206}Pb/^{204}Pb$, $^{207}Pb/^{204}Pb$ and $^{208}Pb/^{204}Pb$ ratios for subsequent modelling are taken

from the BSE curve at 2.6 Ga. μ and κ are selected to satisfy the equations:

$$\left(\frac{^{206}Pb}{^{204}Pb}\right)_{t_0} = \left(\frac{^{206}Pb}{^{204}Pb}\right)_{t_1} + \mu\left(e^{\lambda_{238}t_1} - 1\right) \ldots\ldots\ldots\ldots (1)$$

$$\left(\frac{^{207}Pb}{^{204}Pb}\right)_{t_0} = \left(\frac{^{207}Pb}{^{204}Pb}\right)_{t_1} + \frac{\mu}{137.818}\left(e^{\lambda_{235}t_1} - 1\right) \ldots\ldots (2)$$

$$\left(\frac{^{208}Pb}{^{204}Pb}\right)_{t_0} = \left(\frac{^{208}Pb}{^{204}Pb}\right)_{t_1} + \mu \cdot \kappa\left(e^{\lambda_{232}t_1} - 1\right) \ldots\ldots\ldots (3)$$

Where $\left(\frac{^{20x}Pb}{^{204}Pb}\right)_{t_0}$ is the Pb isotopic ratio at present; $\left(\frac{^{20x}Pb}{^{204}Pb}\right)_{t_1}$ is the Pb isotopic ratio at time t_1; λ_{238}, λ_{235} and λ_{232} are the decay constants for ^{238}U, ^{235}U and ^{232}Th; μ is $^{238}U/^{204}Pb$ at present time and κ is $^{232}Th/^{238}U$ at present time. The Pb isotopic evolution curve for UCC is plotted by forward modelling in 100 million years steps, from the initial Pb isotope ratios at 2.6 Ga, and μ and κ of 10.6 and 4.05 respectively (Fig. 10a, Table S5).

The linear trend shown by Xiaogulihe ultrapotassic rocks (Sun *et al.*, 2014) in Pb isotopic diagrams (Fig. 10b, c, Fig. 11) is defined by a variation much larger than the analytical precision. A similar variation across the direction of mixing between the LOMU component and the SCLM can be seen in Fig. 10 and 11 for the other LOMU type basalts from northeastern China. As the linear trend of Xiaogulihe is at a steep angle to the BSE and UCC curves and the isochrones, it cannot be explained by the evolution of a single source as suggested by Wang et al. (2017). It is more likely that this trend represents mixing between two different LOMU components. Hance, at least two sources are needed to explain the evolution of the two LOMU components. Isochrones connecting the present-day average UCC and the endmembers for the Xiaogulihe-trend intersect the UCC curve at 1.8 and 2.2 Ga which are taken to be the ages of subduction for the two LOMU sources denoted as East Asian low μ 1 and 2 (EALM1 and EALM2, Fig. 10b, c). These sources are then evolved with μ and κ of 2.8 and 4.75 for the 1.8 Ga source and 4.26 and 4.0 for the 2.2 Ga source. The μ and κ are selected so to match the isotopic ratios at the ends of the Xiaogulihe linear trend (Table S5). The East Asia low μ samples can now be explained by mixing between the two LOMU sources and the SCLM (Fig. 10b, c, d).

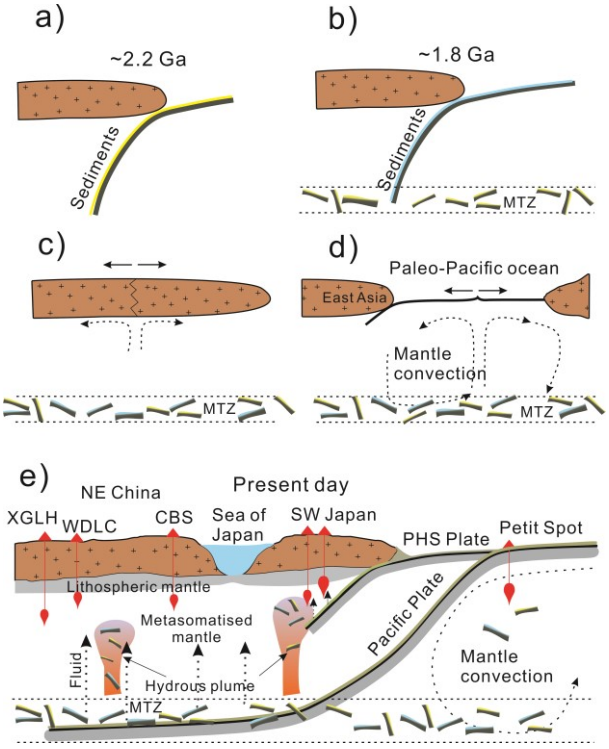

Fig. 12. Schematic diagram representing the evolution of the East Asian low μ component. (a) to (e) represents change in tectonic setting through time. Two different subduction events contributed subducted components which are accumulated at the mantle transition zone and evolve with a low U/Pb ratio up to present time. The two components are assumed to have retained their individual geochemical traits without being homogenized as a single domain. Fluid induced upwelling and melting of the metasomatized mantle generate the low radiogenic Pb bearing alkali basalts in East Asia.

The ages of subduction agree to repeated subduction and collision models established following tectonic, geochronological and petrological studies for the North China Craton during the Paleoproterozoic (Santosh, 2010; Wang *et al.*, 2010; Zhao *et al.*, 2012b), suggesting that repeated subduction of oceanic slab and corresponding sediments are likely to have taken place which subsequently accumulated near the mantle transition zone below the North China Craton. Hydrous upwelling caused by the stagnated Pacific slab causes the remnant fragments of the paleo-slabs to rise, melt, and metasomatise the depleted asthenospheric mantle. A schematic diagram representing the tectonic model is presented in Fig. 12. This model is consistent with previously explored mechanisms of magmatism at the southwest Japan rear arc region and northeast China intraplate region

(Kuritani *et al.*, 2011, 2013, 2017; Sakuyama *et al.*, 2014b, 2014a).

CONCLUSION

This study establishes the presence of a LOMU type mantle component, in the hydrous asthenospheric mantle, below the northern Kyushu area of southwest Japan. The findings of this study can be summarised through the following points.

1. The physicochemical conditions for magmatism for alkali basalts from Kita-Matsuura and Higashi-Matsuura are calculated using mineral chemistry and major elements data. The results suggest that the primary magma is generated in the deep lithosphere to shallow asthenospheric mantle (1.7 - 2.3 GPa), in a hydrous condition (mantle H_2O content 950 – 1600 µg/g) at a mantle potential temperature of ~1300 °C. The Kita-Matsuura basalts are generated in a relatively lower pressure and temperature and higher H_2O content compared to the Higashi-Matsuura basalts.
2. Trace element modelling suggests that the primary basalts can be generated by the melting of the depleted asthenospheric mantle, metasomatised by the melt from an eclogitic component (~15%) present in the mantle. The eclogitic component is modelled as a combination of dehydrated oceanic slab (MORB) containing recycled siliciclastic and carbonate sediments. The pressure-temperature and H_2O content calculated from this model corroborate the values calculated using mineral chemistry and major element data.
3. An isotopic mixing between LOMU type components residing in the asthenospheric mantle, and subcontinental lithospheric mantle xenoliths from Korea is evident from radiogenic Pb-Sr-Nd ratios of Higashi-Matsuura basalts (~3 Ma), indicating a similar Pb isotopic composition of the sub-Kyushu SCLM. However, older (~6 - 8 Ma) alkali basalts about 30 km southeast of this area do not show a LOMU signature which may indicate greater contribution from the SCLM as indicated by a shallower melting depth.
4. A Pb isotope evolution model indicates that two different LOMU components derived from subducted oceanic slabs at 2.2 Ga and 1.8 Ga can explain the variation observed in the East Asian LOMU basalts. These components show a μ of 4.26 and 2.8, and a κ of 4.0 and 4.75 respectively.

ACKNOWLEDGEMENT

We thank Prof. Y. Hayasaka, Prof. K. Das and Dr. T. Hirayama from Hiroshima University for their help in various stages of sampling and data analysis. BD was supported by the Monbukagakusho scholarship during part of the duration of the study. This study was partially supported by HiPeR, which is selected and supported by Hiroshima University. We thank the Hiroshima University for providing the research facilities.

References

Basu, A. R., Wang Junwen, Huang Wankang, Xie Guanghong & Tatsumoto, M. (1991). Major element, REE, and Pb, Nd and Sr isotopic geochemistry of Cenozoic volcanic rocks of eastern China: implications for their origin from suboceanic-type mantle reservoirs. *Earth and Planetary Science Letters* **105**, 149–169. https://doi.org/10.1016/0012-821X(91)90127-4

Birck, J. L. (1986). Precision K-Rb-Sr isotopic analysis: Application to Rb-Sr chronology. *Chemical Geology* **56**, 73–83. https://doi.org/10.1016/0009-2541(86)90111-7

Chang, Q., Shibata, T., Shinotsuka, K., Yoshikawa, M. & Tatsumi, Y. (2002). Precise determination of trace elements in geological standard rocks using inductively coupled plasma mass spectrometry (ICP-MS). *Frontier Research on Earth Evolution* **1**, 357–362.

Chen, H., Xia, Q.-K., Ingrin, J., Jia, Z.-B. & Feng, M. (2015). Changing recycled oceanic components in the mantle source of the Shuangliao Cenozoic basalts, NE China: New constraints from water content. *Tectonophysics* **650**, 113–123. https://doi.org/10.1016/j.tecto.2014.07.022

Chen, H., Xia, Q.-K. K., Ingrin, J., Deloule, E. & Bi, Y. (2017). Heterogeneous source components of intraplate basalts from NE China induced by the ongoing Pacific slab subduction. *Earth and Planetary Science Letters* **459**, 208–220. https://doi.org/10.1016/j.epsl.2016.11.030

Chen, Y., Zhang, Y., Graham, D., Su, S. & Deng, J. (2007). Geochemistry of Cenozoic basalts and mantle xenoliths in Northeast China. *Lithos* **96**, 108–126. https://doi.org/10.1016/j.lithos.2006.09.015

Choi, H. O., Choi, S. H., Lee, Y. S., Ryu, J. S., Lee, D. C., Lee, S. G., Sohn, Y. K. & Liu, J. qi (2020). Petrogenesis and mantle source characteristics of the late Cenozoic Baekdusan (Changbaishan) basalts, North China Craton. *Gondwana Research* **78**,156–171. https://doi.org/10.1016/j.gr.2019.08.004

Choi, S. H., Kwon, S.-T., Mukasa, S. B. & Sagong, H. (2005). Sr–Nd–Pb isotope and trace element systematics of mantle xenoliths from Late Cenozoic alkaline lavas, South Korea. *Chemical Geology* **221**, 40–64. https://doi.org/10.1016/j.chemgeo.2005.04.008

Choi, S. H. & Liu, S.-A. (2022). Zinc isotopic systematics of the Mt. Baekdu and Jeju Island intraplate basalts in Korea, and implications for mantle source lithologies. *Lithos* **416**–**417**, 106659. https://doi.org/10.1016/j.lithos.2022.106659

Choi, S. H., Mukasa, S. B., Kwon, S. T. & Andronikov, A. V. (2006). Sr, Nd, Pb and Hf isotopic compositions of late Cenozoic alkali basalts in South Korea: Evidence for mixing between the two dominant asthenospheric mantle domains beneath East Asia. *Chemical Geology* **232**, 134–151. https://doi.org/10.1016/j.chemgeo.2006.02.014

Compston, W. & Oversby, V. M. (1969). Lead Isotopic Analysis Using a Double Spike. *Journal of Geophysical Research* **74**, 4338–4348. https://doi.org/10.1029/JB074i017p04338

Condie, K. C. (2021). *Earth as an Evolving Planetary System*. Academic Press.

Connelly, J. N. & Bizzarro, M. (2016). Lead isotope evidence for a young formation age of the Earth–Moon system. *Earth and Planetary Science Letters* **452**, 36–43. https://doi.org/10.1016/j.epsl.2016.07.010

Cooper, L. B., Ruscitto, D. M., Plank, T., Wallace, P. J., Syracuse, E. M., & Manning, C. E. (2012). Global variations in H2O/Ce: 1. Slab surface temperatures beneath volcanic arcs. *Geochemistry, Geophysics, Geosystems*. **13**. Q03024, https://doi.org/10.1029/2011GC003902

Cousens, B. L., Allan, J. F. & Gorton, M. P. (1994). Subduction-modified pelagic sediments as the enriched component in back-arc basalts from the Japan Sea: Ocean Drilling Program Sites 797 and 794. *Contributions to Mineralogy and Petrology* **117**,421–434. https://doi.org/10.1007/BF00307275

DePaolo, D. J. (1988). *Neodymium Isotope Geochemistry: an introduction*. *Springer-Verlag*.

DePaolo, D. J. (1981). Trace element and isotopic effects of combined wallrock assimilation and fractional crystallization. *Earth and Planetary Science Letters* **53**, 189–202. https://doi.org/10.1016/0012-821X(81)90153-9

Dey, B., Shibata, T. & Yoshikawa, M. (2023). Sequential Pb-Sr-LREE separation from silicates for isotopic analysis. *Geochemical Journal* **57**, 73–84. https://doi.org/10.2343/geochemj.GJ23006

Douglass, J., Schilling, J. G. & Fontignie, D. (1999). Plume-ridge interactions of the Discovery and Shona mantle plumes with the southern Mid-Atlantic Ridge (40°-55°S). *Journal of Geophysical Research: Solid Earth* **104**, 2941–2962. https://doi.org/10.1029/98JB02642

Eisele, J., Sharma, M., Galer, S. J. G. G., Blichert-Toft, J., Devey, C. W. & Hofmann, A. W. (2002). The role of sediment recycling in EM-1 inferred from Os, Pb, Hf, Nd, Sr isotope and trace element systematics of the Pitcairn hotspot. *Earth and Planetary Science Letters* **196**, 197–212. https://doi.org/10.1016/S0012-821X(01)00601-X

Fang, T., Huang, J. & Zartman, R. E. (2022). Lead isotope evolution during the multi-stage core formation. *Solid Earth Sciences* **7**, 50–59. https://doi.org/10.1016/j.sesci.2021.11.001

Fukao, Y., Obayashi, M., Inoue, H. & Nenbai, M. (1992). Subducting slabs stagnant in the mantle transition zone. *Journal of Geophysical Research* **97**, 4809–4822. https://doi.org/10.1029/91JB02749

Gale, A., Dalton, C. A., Langmuir, C. H., Su, Y. & Schilling, J. G. (2013). The mean composition of ocean ridge basalts. *Geochemistry, Geophysics, Geosystems* **14**, 489–518. https://doi.org/10.1029/2012GC004334

Ghiorso, M. S., Hirschmann, M. M., Reiners, P. W. & Kress, V. C. (2002). The pMELTS: A revision of

MELTS for improved calculation of phase relations and major element partitioning related to partial melting of the mantle to 3 GPa. *Geochemistry, Geophysics, Geosystems* **3**, 1–35. https://doi.org/10.1029/2001GC000217

Hartnady, M. I. H., Kirkland, C. L., Smithies, R. H., Johnson, S. P. & Johnson, T. E. (2022). Pb isotope insight into the formation of the Earth's first stable continents. *Earth and Planetary Science Letters* **578**, 117319. https://doi.org/10.1016/j.epsl.2021.117319

Herzberg, C. & O'hara, M. J. (2002). Plume-Associated Ultramafic Magmas of Phanerozoic Age. *Journal of Petrology* **43**, 1857–1883. https://doi.org/10.1093/petrology/43.10.1857

Hirano, N. & Machida, S. (2022). The mantle structure below petit-spot volcanoes. *Communications Earth and Environment* **3**, 1–11. https://doi.org/10.1038/s43247-022-00438-1

Hoang, N. & Uto, K. (2003). Geochemistry of Cenozoic basalts in the Fukuoka district (northern Kyushu, Japan): Implications for asthenosphere and lithospheric mantle interaction. *Chemical Geology* **198**, 249–268. https://doi.org/10.1016/S0009-2541(03)00031-7

Hoang, N. & Uto, K. (2006). Upper mantle isotopic components beneath the Ryukyu arc system: Evidence for "back-arc" entrapment of Pacific MORB mantle. *Earth and Planetary Science Letters* **249**, 229–240. https://doi.org/10.1016/j.epsl.2006.07.02

Hoang, N., Uto, K., Matsumoto, A. & Itoh, J. (2013). Pleistocene intraplate magmatism in the Goto Islands, SW Japan: Implications for mantle source evolution and regional geodynamics. *Journal of Geodynamics* **68**, 1–17. https://doi.org/10.1016/j.jog.2013.03.002

Hofmann, A. W. W., Jochum, K. P. P., Seufert, M. & White, W. M. M. (1986). Nb and Pb in oceanic basalts: new constraints on mantle evolution. *Earth and Planetary Science Letters* **79**, 33–45. https://doi.org/10.1016/0012-821X(86)90038-5

Huang, Z., Zhao, D., Hasegawa, A., Umino, N., Park, J. H. & Kang, I. B. (2013). Aseismic deep subduction of the Philippine Sea plate and slab window. *Journal of Asian Earth Sciences* **75**, 82–94. https://doi.org/10.1016/j.jseaes.2013.07.002

Ikeda, Y., Nagao, K. & Kagami, H. (2001). Effects of recycled materials involved in a mantle source beneath the southwest Japan arc region: evidence from noble gas, Sr, and Nd isotopic systematics. *Chemical Geology* **175**, 509–522. https://doi.org/10.1016/S0009-2541(00)00354-5

Irvine, T. N. & Baragar, W. R. A. (1971). A Guide to the Chemical Classification of the Common Volcanic Rocks. *Canadian Journal of Earth Sciences* **8**, 523–548. https://doi.org/10.1139/e71-055

Kagami, H., Iwata, M., Iizumi, S. & Nureki, T. (1993). Sr-Nd Isotope Systematics of Xenoliths in Cenozoic Volcanic Rocks from SW Japan. *Proceedings of the Japan Academy, Series B* **69**, 1–6. https://doi.org/10.2183/pjab.69.1

Kamata, H. & Kodama, K. (1999). Volcanic history and tectonics of the Southwest Japan Arc. *The Island Arc* **8**, 393–403. https://doi.org/10.1046/j.1440-1738.1999.00241.x

Kanazawa, T., Sager, W. & Escutia, C. (2001). Explanatory Notes. *Proceedings of the Ocean Drilling Program, Initial Reports Volume 191*, 46.

Kelley, K. A., Plank, T., Grove, T. L., Stolper, E. M., Newman, S. & Hauri, E. (2006). Mantle melting as a function of water content beneath back-arc basins. *Journal of Geophysical Research: Solid Earth* **111**, 9208. https://doi.org/10.1029/2005JB003732

Kim, J. I., Choi, S. H., Koh, G. W., Park, J. B. & Ryu, J. S. (2019). Petrogenesis and mantle source characteristics of volcanic rocks on Jeju Island, South Korea. *Lithos* **326–327**, 476–490. https://doi.org/10.1016/j.lithos.2018.12.034

Kimura, J. & Kawabata, H. (2015). Ocean Basalt Simulator version 1: Trace element mass balance in adiabatic melting of a pyroxenite-bearing peridotite. *Geochemistry, Geophysics, Geosystems* **16**, 267–300. https://doi.org/10.1002/2014GC005606

Klemme, S. & O'Neill, H. S. C. (2000). The near-solidus transition from garnet lherzolite to spinel lherzolite. *Contributions to Mineralogy and Petrology* **138**, 237–248. https://doi.org/10.1007/s004100050560

Kuritani, T., Kimura, J.-I., Miyamoto, T., Wei, H., Shimano, T., Maeno, F., Jin, X. & Taniguchi, H.

(2009). Intraplate magmatism related to deceleration of upwelling asthenospheric mantle: Implications from the Changbaishan shield basalts, northeast China. *Lithos* **112**, 247–258. https://doi.org/10.1016/j.lithos.2009.02.007

Kuritani, T., Kimura, J.-I., Ohtani, E., Miyamoto, H. & Furuyama, K. (2013). Transition zone origin of potassic basalts from Wudalianchi volcano, northeast China. *Lithos* **156**–**159**, 1–12. https://doi.org/10.1016/j.lithos.2012.10.010

Kuritani, T., Ohtani, E. & Kimura, J. (2011). Intensive hydration of the mantle transition zone beneath China caused by ancient slab stagnation. *Nature Geoscience* **4**, 713–716. https://doi.org/10.1038/ngeo1250

Kuritani, T., Sakuyama, T., Kamada, N., Yokoyama, T. & Nakagawa, M. (2017). Fluid-fluxed melting of mantle versus decompression melting of hydrous mantle plume as the cause of intraplate magmatism over a stagnant slab: Implications from Fukue Volcano Group, SW Japan. *Lithos* **282**–**283**, 98–110. https://doi.org/10.1016/j.lithos.2017.02.011

Kuritani, T., Xia, Q.-K. Q.-K., Kimura, J.-I. J.-I., Liu, J., Shimizu, K., Ushikubo, T., Zhao, D., Nakagawa, M. & Yoshimura, S. (2019). Buoyant hydrous mantle plume from the mantle transition zone. *Scientific Reports* **9**, 6549. https://doi.org/10.1038/s41598-019-43103-y

Le Bas, M. J., Le Maitre, R. W., Streckeisen, A. & Zanettin, B. (1986). A chemical classification of volcanic rocks based on the total alkali-silica diagram. *Journal of Petrology* **27**, 745–750. https://doi.org/10.1093/petrology/27.3.745

Lee, C. T. A., Luffi, P., Plank, T., Dalton, H. & Leeman, W. P. (2009). Constraints on the depths and temperatures of basaltic magma generation on Earth and other terrestrial planets using new thermobarometers for mafic magmas. *Earth and Planetary Science Letters* **279**, 20–33. https://doi.org/10.1016/j.epsl.2008.12.020

Li, S. G., Yang, W., Ke, S., Meng, X., Tian, H., Xu, L., He, Y., Huang, J., Wang, X.C., Xia, Q. & Sun, W. (2017). Deep carbon cycles constrained by a large-scale mantle Mg isotope anomaly in eastern China. *National Science Review* **4**, 111–120. https://doi.org/10.1093/nsr/nww070

Li, T. (2010). The principal characteristics of the lithosphere of China. *Geoscience Frontiers* **1**, 45–56. https://doi.org/10.1016/j.gsf.2010.08.005

Liu, J. Q., Chen, L. H., Wang, X. J., Zhong, Y., Yu, X., Zeng, G. & Erdmann, S. (2017). The role of melt-rock interaction in the formation of Quaternary high-MgO potassic basalt from the Greater Khingan Range, northeast China. *Journal of Geophysical Research: Solid Earth* **122**, 262–280. https://doi.org/10.1002/2016JB013605

Liu, J., Hirano, N., Machida, S., Xia, Q., Tao, C., Liao, S., Liang, J., Li, W., Yang, W., Zhang, G. & Ding, T. (2020a). Melting of recycled ancient crust responsible for the Gutenberg discontinuity. *Nature Communications* **11**, 1–9. https://doi.org/10.1038/s41467-019-13958-w

Liu, S. A. & Li, S. G. (2019). Tracing the Deep Carbon Cycle Using Metal Stable Isotopes: Opportunities and Challenges. *Engineering* **5**, 448–457. https://doi.org/10.1016/j.eng.2019.03.007

Liu, S. A., Wang, Z. Z., Yang, C., Li, S. G. & Ke, S. (2020b). Mg and Zn Isotope Evidence for Two Types of Mantle Metasomatism and Deep Recycling of Magnesium Carbonates. *Journal of Geophysical Research: Solid Earth* **125**, e2020JB020684. https://doi.org/10.1029/2020JB020684

Machida, S., Hirano, N. & Kimura, J. I. (2009). Evidence for recycled plate material in Pacific upper mantle unrelated to plumes. *Geochimica et Cosmochimica Acta* **73**, 3028–3037. https://doi.org/10.1016/j.gca.2009.01.026

Mahony, S. H., Wallace, L. M., Miyoshi, M., Villamor, P., Sparks, R. J. & Hasenaka, T. (2011). Volcano-tectonic interactions during rapid plate-boundary evolution in the Kyushu region, SW Japan. *Bulletin of the Geological Society of America* **123**, 2201–2223. https://doi.org/10.1130/B30408.1

Maltese, A. & Mezger, K. (2020). The Pb isotope evolution of Bulk Silicate Earth: Constraints from its accretion and early differentiation history. *Geochimica et Cosmochimica Acta* **271**, 179–193. https://doi.org/10.1016/j.gca.2019.12.021

Michael, P. (1995). Regionally distinctive sources of depleted MORB: Evidence from trace elements and H2O. *Earth and Planetary Science Letters* **131**,

301–320. https://doi.org/10.1016/0012-821X(95)00023-6

Millot, R., Allègre, C.-J. J., Gaillardet, J. & Roy, S. (2004). Lead isotopic systematics of major river sediments: a new estimate of the Pb isotopic composition of the Upper Continental Crust. *Chemical Geology* **203**, 75–90. https://doi.org/10.1016/j.chemgeo.2003.09.002

Nakamura, E., McDougall, I. & Campbell, I. H. (1986). K-Ar ages of basalts from the Higashi-Matsuura district, northwestern Kyushu, Japan and regional geochronology of the Cenozoic alkaline volcanic rocks in eastern Asia. *Geochemical Journal* **20**, 91–99. https://doi.org/10.2343/geochemj.20.91

Pearce, J. A. (2008). Geochemical fingerprinting of oceanic basalts with applications to ophiolite classification and the search for Archean oceanic crust. *Lithos* **100**, 14–48. https://doi.org/10.1016/j.lithos.2007.06.016

Pearce, J. A. & Cann, J. R. (1973). Tectonic setting of basic volcanic rocks determined using trace element analyses. *Earth and Planetary Science Letters* **19**, 290–300. https://doi.org/10.1016/0012-821X(73)90129-5

Pearce, T. H. (1978). Olivine fractionation equations for basaltic and ultrabasic liquids. *Nature* **276**, 771–774. https://doi.org/10.1038/276771a0

Perinelli, C., Mollo, S., Gaeta, M., De Cristofaro, S. P., Palladino, D. M., Armienti, P., Scarlato, P. & Putirka, K. D. (2016). An improved clinopyroxene-based hygrometer for Etnean magmas and implications for eruption triggering mechanisms. *American Mineralogist* **101**, 2774–2777. https://doi.org/10.2138/am-2016-5916

Plank, T. (2014). The Chemical Composition of Subducting Sediments. *Treatise on Geochemistry*. Elsevier, 607–629. https://doi.org/10.1016/B978-0-08-095975-7.00319-3

Putirka, K. D. (2008). Thermometers and barometers for volcanic systems. *Reviews in Mineralogy and Geochemistry* **69**, 61–120. https://doi.org/10.2138/rmg.2008.69.3

Richard, G. C. & Iwamori, H. (2010). Stagnant slab, wet plumes and Cenozoic volcanism in East Asia. *Physics of the Earth and Planetary Interiors* **183**, 280–287. https://doi.org/10.1016/j.pepi.2010.02.009

Roeder, P. L. & Emslie, R. F. (1970). Olivine-liquid equilibrium. *Contributions to Mineralogy and Petrology* **29**, 275–289 https://doi.org/10.1007/BF00371276

Rudnick, R. L., Goldstine, S. L., Goldstein, S. L., Goldstine, S. L., Goldstein, S. L., Goldstine, S. L. & Goldstein, S. L. (1990). The Pb isotopic compositions of lower crustal xenoliths and the evolution of lower crustal Pb. *Earth and Planetary Science Letters* **98**, 192–207. https://doi.org/10.1016/0012-821X(90)90059-7

Saitoh, Y., Ishikawa, T., Tanimizu, M., Murayama, M., Ujiie, Y., Yamamoto, Y., Ujiie, K. & Kanamatsu, T. (2015). Sr, Nd, and Pb isotope compositions of hemipelagic sediment in the Shikoku Basin: Implications for sediment transport by the Kuroshio and Philippine Sea plate motion in the late Cenozoic. *Earth and Planetary Science Letters* **421**, 47–57. https://doi.org/10.1016/j.epsl.2015.04.001

Sakuyama, T., Tian, W., Kimura, J.I., Fukao, Y., Hirahara, Y., Takahashi, T., Senda, R., Chang, Q., Miyazaki, T., Obayashi, M. and Kawabata, H. (2013). Melting of dehydrated oceanic crust from the stagnant slab and of the hydrated mantle transition zone: Constraints from Cenozoic alkaline basalts in eastern China. *Chemical Geology* **359**, 32–48. https://doi.org/10.1016/j.chemgeo.2013.09.012

Sakuyama, T., Nagaoka, S., Miyazaki, T., Chang, Q., Takahashi, T., Hirahara, Y., Senda, R., Itaya, T., Kimura, J.I. and Ozawa, K. (2014a). Melting of the Uppermost Metasomatized Asthenosphere Triggered by Fluid Fluxing from Ancient Subducted Sediment: Constraints from the Quaternary Basalt Lavas at Chugaryeong Volcano, Korea. *Journal of Petrology* **55**, 499–528. https://doi.org/10.1093/petrology/egt074

Sakuyama, T., Nakai, S., Yoshikawa, M., Shibata, T. & Ozawa, K. (2014b). Progressive interaction between dry and wet mantle during high-temperature diapiric upwelling: Constraints from cenozoic kita-matsuura intraplate basalt province, Northwestern Kyushu, Japan. *Journal of Petrology* **55**, 1083–1128. https://doi.org/10.1093/petrology/egu020

Sakuyama, T., Ozawa, K., Sumino, H. & Nagao, K. (2009). Progressive melt extraction from upwelling mantle constrained by the kita-matsuura basalts in NW Kyushu, SW Japan. *Journal of Petrology* **50**, 725–779. https://doi.org/10.1093/petrology/egp018

Salters, V. J. M. & Stracke, A. (2004). Composition of the depleted mantle. *Geochemistry, Geophysics, Geosystems* **5**, Q05B07. https://doi.org/10.1029/2003GC000597

Santosh, M. (2010). Assembling North China Craton within the Columbia supercontinent: The role of double-sided subduction. *Precambrian Research* **178**, 149–167. https://doi.org/10.1016/j.precamres.2010.02.003

Senda, R., Tanaka, T. & Suzuki, K. (2007). Os, Nd, and Sr isotopic and chemical compositions of ultramafic xenoliths from Kurose, SW Japan: Implications for contribution of slab-derived material to wedge mantle. *Lithos* **95**, 229–242. https://doi.org/10.1016/j.lithos.2006.07.014

Shi, J., Zeng, G., Chen, L., Wang, X., Liu, J., Xie, L., Yang, Y. & Zhang, H. (2023). Lithology of EM1 Reservoir Revealed by Fe Isotopes of Continental Potassic Basalts. *Journal of Geophysical Research: Solid Earth* **128**, 1–17. https://doi.org/10.1029/2022JB025133

Shibata, T., Yoshikawa, M., Itoh, J., Ujike, O., Miyoshi, M. & Takemura, K. (2014). Along-arc geochemical variations in Quaternary magmas of northern Kyushu Island, Japan. *Geological Society, London, Special Publications*. **385**, 15–29. https://doi.org/10.1144/SP385.13

Stacey, J. S. & Kramers, J. D. (1975). Approximation of terrestrial lead isotope evolution by a two-stage model. *Earth and Planetary Science Letters* **26**, 207–221. https://doi.org/10.1016/0012-821X(75)90088-6

Sugimoto, T., Shibata, T., Yoshikawa, M. & Takemura, K. (2006). Sr-Nd-Pb isotopic and major and trace element compositions of the Yufu-Tsurumi volcanic rocks: implications for the magma genesis of the Yufu-Tsurumi volcanoes, northeast Kyushu, Japan. *Journal of Mineralogical and Petrological Sciences* **101**, 207–275. https://doi.org/10.2465/jmps.101.270

Sumino, H., Nakai, S. N. I., Nagao, K. & Notsu, K. (2000). High ^{3}He/4He ratio in xenoliths from Takashima: Evidence for plume type volcanism in southwestern Japan. *Geophysical Research Letters* **27**, 1211–1214. https://doi.org/10.1029/1999GL008438

Sun, S. -s. & McDonough, W. F. (1989). Chemical and isotopic systematics of oceanic basalts: implications for mantle composition and processes. *Geological Society, London, Special Publications*. **42**, 313–345. https://doi.org/10.1144/GSL.SP.1989.042.01.19

Sun, Y., Teng, F. Z., Ying, J. F., Su, B. X., Hu, Y., Fan, Q. C. & Zhou, X. H. (2017). Magnesium Isotopic Evidence for Ancient Subducted Oceanic Crust in LOMU-Like Potassium-Rich Volcanic Rocks. *Journal of Geophysical Research: Solid Earth* **122**, 7562–7572. https://doi.org/10.1002/2017JB014560

Sun, Y., Ying, J., Zhou, X., Shao, J., Chu, Z. & Su, B. (2014). Geochemistry of ultrapotassic volcanic rocks in Xiaogulihe NE China: Implications for the role of ancient subducted sediments. *Lithos*. **208**, 53–66.https://doi.org/10.1002/2017JB014560

Takai, Y. & Uehara, S. (2012). Rhabdophane-(Y), YPO4·H2O, a new mineral in alkali olivine basalt from Hinodematsu, Genkai-cho, Saga Prefecture, Japan. *Journal of Mineralogical and Petrological Sciences* **107**, 110–113. https://doi.org/10.2465/jmps.111020j

Tatsumi, Y., Sakuyama, M., Fukuyama, H. & Kushiro, I. (1983). Generation of arc basalt magmas and thermal structure of the mantle wedge in subduction zones. *Journal of Geophysical Research: Solid Earth* **88**, 5815–5825. https://doi.org/10.1029/JB088iB07p05815

Tatsumoto, M. (1969). Lead isotopes in volcanic rocks and possible ocean-floor thrusting beneath island arcs. *Earth and Planetary Science Letters* **6**, 369–376. https://doi.org/10.1016/0012-821X(69)90187-3

Tatsumoto, M. & Nakamura, Y. (1991). DUPAL anomaly in the Sea of Japan: Pb, Nd, and Sr isotopic variations at the eastern Eurasian continental margin. *Geochimica et Cosmochimica Acta* **55**, 3697–3708. https://doi.org/10.1016/0016-7037(91)90068-G

Uto, K., Hoang, N. & Matsui, K. (2004). Cenozoic lithospheric extension induced magmatism in Southwest Japan. *Tectonophysics* **393**, 281–299. https://doi.org/10.1016/j.tecto.2004.07.039

Wang, X.-J., Chen, L.-H., Hofmann, A. W., Mao, F.-G., Liu, J.-Q., Zhong, Y., Xie, L.-W. & Yang, Y.-H. (2017). Mantle transition zone-derived EM1 component beneath NE China: Geochemical evidence from Cenozoic potassic basalts. *Earth and Planetary Science Letters* **465**, 16–28. https://doi.org/10.1016/j.epsl.2017.02.028

Wang, X., Hou, T., Wang, M., Zhang, C., Zhang, Z., Pan, R., Marxer, F. & Zhang, H. (2021). A new clinopyroxene thermobarometer for mafic to intermediate magmatic systems. *European Journal of Mineralogy* **33**, 621–637. https://doi.org /10.5194/ejm-33-621-2021

Wang, Z., Wilde, S. A. & Wan, J. (2010). Tectonic setting and significance of 2.3-2.1 Ga magmatic events in the Trans-North China Orogen: New constraints from the Yanmenguan mafic-ultramafic intrusion in the Hengshan-Wutai-Fuping area. *Precambrian Research* **178**, 27–42. https://doi.org/10.1016/j.precamres.2010.01.005

Wei, F., Pan, B. & Xu, J. (2021). Sr-Nd-Pb-Ca Isotopes of Holocene Basalts from Jingpohu, NE China: Implications for the Origin of Their Enriched Mantle Signatures. *Minerals*. **11**, 790. https://doi.org/10.3390/min11080790

Weng, B.-Y., Hong, L.-B., Zhang, Y.-H., Zhang, L., Xu, Y.-G., Yuan, C. & He, P.-L. (2022). Petrological evidence of an anhydrous carbonatitic peridotite source for the Xiaogulihe ultrapotassic volcanic rocks, northeastern China. *Lithos* **426**–**427**, 106776. https://doi.org/10.1016/j.lithos.2022. 106776

Wilson, M. (Ed.). (1989). Igneous petrogenesis. *Dordrecht: Springer Netherlands*.

Workman, R. K. & Hart, S. R. (2005). Major and trace element composition of the depleted MORB mantle (DMM). *Earth and Planetary Science Letters*. Elsevier **231**, 53–72. https:// doi.org/10.1016/j.epsl.2004.12.005

Yoshikawa, M., Arai, S., Ishida, Y., Tamura, A. & Shimizu, Y. (2010). Trace element and Sr-Nd isotopic features of ultramafic xenoliths from Kurose, Southwest Japan. *Journal of Mineralogical and Petrological Sciences* **105**, 346–351. https://doi.org/10.2465/jmps.100622b

Zhang, M., Suddaby, P., Thompson, R. N., Thirlwall, M. F. & Menzies, M. A. (1995). Potassic volcanic rocks in NE China: Geochemical constraints on mantle source and magma genesis. *Journal of Petrology* **36**, 1275–1303. https://doi.org /10.1093/petrology/36.5.1275

Zhao, D., Yanada, T., Hasegawa, A., Umino, N. & Wei, W. (2012a). Imaging the subducting slabs and mantle upwelling under the Japan Islands. *Geophysical Journal International* **190**, 816–828. https://doi.org/10.1111/j.1365-246X.2012.055 50.x

Zhao, G., Cawood, P. A., Li, S., Wilde, S. A., Sun, M., Zhang, J., He, Y. & Yin, C. (2012b). Amalgamation of the North China Craton: Key issues and discussion. *Precambrian Research* **222**–**223**, 55–76. https://doi.org/10.1016 /j.precamres.2012.09.016

Zindler, A. & Hart, S. (1986). Chemical Geodynamics. *Annual Review of Earth and Planetary Sciences* **14**, 493–571. https://doi.org/10.1146/annurev.earth. 14.1.493

Zou, H., Reid, M. R., Liu, Y., Yao, Y., Xu, X. & Fan, Q. (2003). Constraints on the origin of historic potassic basalts from northeast China by U–Th disequilibrium data. *Chemical Geology* **200**, 189–201. https://doi.org/10.1016/S0009-2541(03) 00188-8